Development of Sensor Technology to Facilitate In-situ Measurement of Damage in Composite Materials for Spacecraft Applications (final report)

M.C.Mowlem

University of Southampton, SO17 1BJ, UK

| Engineering Materials

| Optoelectronics

Report No. AC/RS/MM/99/05/269

Development of Sensor Technology to Facilitate In-situ Measurement of Damage in Composite Materials for Spacecraft Applications

Mr. M Mowlem, Dr J. Dakin, Dr A. Chambers, Dr M. Singh.

1 Preamble

1.1 Abstract

This document is a report on the work undertaken at the University of Southampton to develop sensor technology to facilitate in-situ measurement of damage in composite materials for spacecraft applications during the last fourteen months.

Work has concentrated on the investigation and evaluation of Bragg grating based optical strain sensors for this application. The results from sensor testing with an existing sensor interrogation technology (produced by H.Gieger[XXX]) show that this system is capable of detecting impact damage from 11.8-Joule impact even when sensors are distant from the impact site. In addition sensor-reading transients (strain and temperature) are seen which could allow the elucidation of information pertaining to the nature of the impact.

Despite these positive results it is understood that this interrogation technology is at present sub-optimal. Therefore, considerable effort has been expended developing a new interrogation technology. In terms of the initial brief (to enable damage detection and measurement) an improved interrogation system would allow better resolution for damage characterisation and detection of smaller defects. In addition such a system may be better able to characterise impacts. This is seen as the logical extension of the project. High-speed digital photography of the impacts has been used to identify the nature of post impact vibration and acoustic response of CFRP. These results indicate that the recording of sensor transients with a higher sampling rate could provide further information to characterise impacts.

1.2 Objectives

The object of this project was to develop and characterise a sensor for the in-situ measurement of impact damage in composite materials used in spacecraft applications. This was broken down as follows:

1.2.1 Development of sensor technology

- Development of Wave Domain Multiplexing (WDM) interrogation system
- Development of a high accuracy Time Domain Multiplexing (TDM) interrogation system.

1.2.2 Characterisation of sensor technology

- Assessment of Bragg grating array effectiveness for the measurement of residual strain fields produced by impact damage.
- Assessment of Bragg grating array effectiveness for the measurement of stiffness matrix modification produced by impact damage.
- Assessment of sensor effectiveness for the measurement of dynamic strain caused by impacts.
- Study of impact damage mechanisms in composite materials and their effect on measured properties.
- Relation of sensor readings to impact damage.

1.3 Project Achievements

1.3.1 Improvement of TDM system

Two major faults have been detected and remedied in the existing TDM interrogation system. The modifications to the hardware and software necessary to effect this improvement are detailed in section XXXXXX.

The functionality of the TDM system has also been extended to allow the measurement and logging of dynamic strain at a single sensor with a sampling frequency of 200Hz (see XXXXX).

1.3.2 Execution of medium velocity (11.8 joule, 225 m/s) impact experiments

A series of impact experiments have been conducted using a medium speed impact rig with projectiles fired from and airgun. Sensor loaded test panels of unidirectional CFRP and CARALL have both been tested with impact events recorded using high-speed digital photography (40500 frames/sec). These experiments and the results are described in section XXXXXX.

1.3.3 Development of alternative interrogation technology

The majority of the research effort has been concentrated in the development of an alternative interrogation technology as described in section 5. The attractions of WDM (which this system may offer) and the promise of increased interrogation accuracy produced the motivation for this activity. A discussion of the relative merits of WDM and TDM are outlined in section 4.2. At the time of writing the new interrogation is not yet fully operational. However all the perceived technical hurdles have been overcome and initial component performance is in line with the capability and resolution predicted in section 2.

1.4 Report Structure

The remainder of this report is divided into two sections. The first deals with the examination of current sensor and interrogation technology to assess its suitability for this application. This was achieved by the execution of a number of impact experiments which are described below. The second details the steps that have been made to improve and develop interrogation technologies.

2 Impact Experiments

2.1 Experimental aims

In order to assess the suitability of Bragg grating based sensor arrays for impact damage measurement and to evaluate the present interrogation system a series of impact experiments were conducted. The aim of these experiments was to meet the objectives set out in XXXXX namely to evaluate this systems ability to measure changes in residual strain, stiffness of CFRP pre and post impact and to monitor dynamic strain during impact events. Such capability would enable this sensor to be used as a damage sensor in this application.

The conditions encountered by CFRP structures in spacecraft applications are difficult to mimic in terrestrial experiments. Impact velocities of 20km/s are not uncommon whilst particles of only a few micrograms are the norm. Whilst facilities do exist that are capable of producing particles of the required size and velocity it was felt that at this evaluation stage it was more suitable to concentrate on the performance of the sensors rather than exactly reproduce the conditions of space. An air rifle was chosen as the impact particle generator as this option allowed relatively high-speed (225m/s) and low mass (0.5g) particles to be produced. Whilst the energy of these impacts exceeds that expected from small

micrometeoroids and debris particles by an order of magnitude the resultant damage is consistent to that seen with higher speed impacts. At locations distant from the impact site the residual strains would be small and were felt to compare to an order of magnitude to the strains that would be observed by a smaller but closer impact. An air rifle also has the advantage of producing particles that can reliably hit a small target at a consistent angle which is certainly not true for some high speed particle generation systems.

2.2 Experimental Method

The sensor-loaded panels used in this experiment contained an array of forty Bragg grating strain sensors embedded in the centre of a 4 ply unidirectional CFRP (913HTA) laminate structure with a 0.6 fibre / volume fraction. The laminate was cured at 130 °C in an autoclave and had a thickness of 0.5mm. These panels originally formed the central element of Carbon fibre Reinforced Aluminium laminates (CARALL) used for fatigue assessment by MM Singh et al. [6] and were used to reduce the lead time and cost of the experiments. Three panels were investigated, one with both Aluminium layers (8090 (0.45mm)) removed (panel C), the others with one skin removed (panels 8h13 and 8H9). Although materials structures such as these are not used extensively in spacecraft applications it was felt that they would provide adequate test specimens to demonstrate this impact damage assessment technology. The gratings were etched onto five optical fibre lines at 1,2,3,4,6,8,12 and 20 mm from the central x-axis (transverse axis) of the test panels. The lines were placed at 20,25,30,35 and 40mm from the centre of the panels parallel to the y-axis (longitudinal axis).

Impinging particles were produced by an air rifle, which produced an impact velocity of 225ms with a 0.0005kg, 4.5mm diameter particle (11.8 J impact). Impact location was varied for each panel and repeated until a residual strain was observed. Panel C required 2 impacts before residual strains were observed.

During impact events a single strain sensor was monitored with a sampling rate of 200Hz to examine the sensors ability to record dynamic strain effects. High-speed digital photography (40500 frames/s) was used to record each impact event and the subsequent vibration. The images produced gave a valuable insight into the response of the panel, the nature of the damage mechanism and the readings recorded by the strain sensor.

Residual strains and stiffness changes were measured by the evaluation of the strain versus load characteristics of the panels pre and post impact. This was achieved by was loading each panel to 10kN in 2kN increments in a servo-hydraulic machine with all strain sensor outputs recorded at each load both before and after impact.

A number of sources of systematic error exist in the TDM interrogation system. Perhaps the most significant of which is the dependence of the AOTF centre frequency for a given RF drive frequency on temperature. This temperature dependence has a critical effect on the output of this interrogation system as the mean RF drive frequency is measured and used directly to locate the bragg grating sensor wavelength. This effect is removed by the use of reference gratings which are held at a constant strain and temperature. This arrangement insures that the reflected wavelengths from these gratings are constant and can be used to calibrate the AOTF. In addition the sensors exhibit a small temperature dependence (approximately 0.01 nm/°C which gives a strain error of 0.008$\mu\varepsilon$/°C [3]). However this error is considerably smaller than the resolution limit of the system and was therefore ignored in this experiment. If the resolution of the interrogation system were to improve additional reference gratings (constant strain and ambient temperature) could be used to remove sensor temperature effects assuming that the sensors in the test panels remained at ambient temperature.

2.3 RESULTS AND DISCUSSION

2.3.1 Observed damage

After each impact on panel C a 3.5mm width of the material was removed (fibre and matrix failure) along the length of the panel. A region of visible delamination was also created 1mm either side of this void. The 2nd impact which resulted in residual strains was located 4mm from the first optical fibre in the transverse direction and adjacent to the third Bragg grating in the longitudinal direction.

Panels 8h13 and 8h9 exhibited much less damage to the carbon layer. A 4mm hole was produced in both panels with 8-10mm long parallel cracks extending from both sides of the tangent of the impact whole in the longitudinal orientation. The aluminium layer at the rear of the specimen exhibited a 30mm diameter heavily deformed region (completely delaminated from the carbon layer) with a rupture resulting in a 15mm crack through which the particle had escaped. The impact for panel 8h9 was located 29mm from the first optic line and parallel with the last grating in each line. The impact on panel 8H13 was 9mm from the first optic line and 15mm from the first grating (i.e. parallel to a line between the penultimate and last grating) in the longitudinal direction.

The damage observed was consistent with the differing properties afforded by the two types of test specimen. Whilst the addition of the aluminium layer greatly increased the strength of the material particularly in the transverse direction the increase in ductility which this configuration offered resulted in more energy absorption and hence damage.

2.3.2 Sensor Readings

Residual Strain information

Similarly the strain sensor readings were consistent with the observed damage for all of the panels. The residual strain observed by all sensors in both 8h9 (fig.1.) and 8h13 (fig.2.) were larger than those recorded by any of the sensors in panel C (fig.3.). This is consistent with the stresses induced by the plastic deformation of the 8090 aluminium layer present in panels 8h9 and 8h13. A variation in residual strain can also be seen with location for each panel this is illustrated by the slopes on the surfaces shown in figures 4 and 5 (impacts are nearest the first line). A full analysis of the expected residual strain field is yet to be completed but many of the results appear consistent with the expectation that residual strains are greater closest to each impact. There is little appreciable change in stiffness observed due to the impact damage created.

Strain transient information

Detailed strain transient information is limited due to the relatively low sampling rate of the interrogation system. Fig.6. shows the transient response of grating 8 on the first line of the sensor array during the impact of the panel. The creation of a large residual strain can clearly be seen. However, tracing of the immediate post impact transient is limited although some post impact vibration is detected. Post impact vibration at approximately 3kHz was observed using a high-speed digital camera. A longer time-constant variation was also observed post-impact. This is probably due to the heating and cooling of the aluminium post impact, which creates thermal strain. This effect is not due to the heating of the sensor directly and was much smaller for panel C.

High Speed Digital Photography

Animation of the images retrieved using the high speed digital camera is the most satisfactory method of viewing these results. The high frame rate used by this equipment necessitates that the image recorded is both small and of low resolution (64X64 pixels). However when animated at a suitable frame rate (5-100 frames per second) the response of the panels can be seen clearly. Despite the poor translation of this medium into still images a number of features can be discerned in figures 7-21.

Figs. 7-14 show the first seven frames of an test impact onto a 2mm 8090 Al alloy sheet of the same dimensions as the test panels. The white arrows track the progression of the initial impact wave (this is not an acoustic wave in the material as it is only moving at approximately 40m/s) whilst the black arrows chart the passage of two of the many particles ejected from the

impact site. These are believed to be metal oxides from the surface of the plate and the impinging particle.

Figs. 15-21 show a number of frames selected from the record of the first impact on panel C. The first three frames chart the movement of a group of fractured fibres as they are flung out of the material by the post impact vibration and then return in the course of approximately 3ms. Another vibration can be seen in the final three frames. The opening and closing of the delaminated crack can clearly be seen to move with a half cycle duration of approximately 1ms.

A number of other interesting panel responses are clearly visible in the animation of the complete record of each impact. Of particular interest is the mass of vibration that occurs for up to 10ms after an impact event. Although the sensors are mounted on the neutral axis it is expected that higher resolution in the interrogation system would allow a closer examination of this vibration and may even enable the characterisation of impacts from its nature.

3 Interrogation System Development

3.1 Sensing concept

The sensing concept is based on measurement of the peak wavelength of light reflected from in-fibre Bragg gratings. Each grating reflects a gaussian power distribution in the wavelength domain with a central peak at a characteristic wavelength. This characteristic wavelength depends on both the mean velocity of light in the fibre core and the spatial period of refractive index changes in the fibre material in the region of the grating. These refractive index changes are induced in a fibre by the action of phase controlled ultraviolet laser impingement and can be controlled in size spacing and intensity to give a range of sensor properties.

If the physical structure of the fibre containing the grating is disrupted by changes in strain (or temperature), the result is a change in the mean refractive index and in the spatial period of the refractive index changes, resulting in a corresponding change in the wavelength of the reflected light. In bare fibre, this effect has been found to result in wavelength shifts of the order of 1.2 nm / $\mu\varepsilon$. [3]

Optical fibres containing Bragg grating sensors can be included within the matrix of fibre reinforced plastics with little detriment to their physical properties (due to their relatively small diameter (typically 126μm)) and offer good mechanical coupling. Each optical fibre line can contain a number of discreet grating based sensors with as little as 1mm separating each grating. The length of each sensor can be reduced to the sub-millimetre but a loss in reflected power is observed with decreasing sensor length.

The interrogation technology employed produces a limit on the number of sensors in each fibre due to resolution and speed problems. If sensor peak wavelengths are too close (closer than the filter band width) then cross talk can be induced, in addition most interrogation systems use a single optical filter to sample a reflected power spectrum thus additional sensors reduce the time available to sample each peak.

An array of Bragg grating based sensors placed in the CFRP structure enables accurate strain profiling of the material pre-impact and post-impact. This is achieved by recording the centre wavelength of each grating (whose locations are known) in both states. This strain information can then be related to the observed damage and the sensor calibrated to measure damage in remote locations. Dynamic strain information can give further information to enable the prediction of impact damage.

3.2 Advantages of TDM and WDM

In TDM each grating is interrogated individually in the time domain, the next grating is then measured after a specified time period. This dictates that TDM is only capable of measuring static (residual) strain patterns and dynamic strain in one sensor. In WDM all sensors are interrogated simultaneously in the time domain but are resolved individual in the wave domain. True WDM allows the resolution of the strain in any sensor at any time. If WDM is achieved dynamic strain in more than one sensor can be recorded.

In real systems there is a limit to the sampling rate of any data and hence both WDM and TDM systems have a dynamic strain frequency resolution limit. Conversely if a TDM system is sufficiently agile and can interrogate a grating in a very short period of time then it may achieve pseudo WDM by dithering between the gratings at a rate higher than that of the dynamic strain frequency.

The advantage of WDM for this application is that it can offer high frequency dynamic strain information from a number of sensors. This would enable data to be gathered on any impact within the sensitivity of each sensor over the whole test panel surface. Hypervelocity and micrometeoroid impacts with particles of small mass would produce large dynamic strains in a CFRP panel but would create only localised damage [1]. Such localised damage may produce only very small residual strains at sensor locations and hence a system utilising residual strain information may have a relatively high threshold of particle size of which it can measure the associated damage. Dynamic strain information however could enable the prediction of the damage caused by the impact of these small particles even if no residual strain information were available.

3.3 Existing TDM system

As a result of collaboration between the Optoelectronics Research Centre (ORC) and the Department of Engineering Materials at the University of Southampton a TDM system exists [2] for the measurement of fatigue damage in CARALL. The method of interrogation utilises active feedback control to lock-on to the centre wavelength of the grating monitored at any given time.

For this system the maximum dynamic strain rate is 100Hz (for one grating), the settling time 1mS and the maximum resolution 0.18 $\mu\varepsilon/\sqrt{HZ}$. This system is therefore, capable of measuring the development of slow damage mechanisms such as fatigue or of measuring the residual strain left by mechanisms with a shorter duration such as impact damage.

Two major faults have been identified and remedied in the TDM system. The first problem relates to a phase error between two PC supplied signals. To locate a peak, the AOTF has its centre wavelength toggled between two points either side of the reflected peak. If the reflected power at these wavelengths is identical then the peak is then located at the median of these two points. If this is not the case the difference between these reflected powers is used to generate an error signal which is fed back to move the centre wavelength of the AOTF to the correct position. The generation of this error signal requires that the phase of the AOTF toggling signal (signal1) and the signal passed to the error signal production electronics (signal2) is preserved at all times. This enables the correct reflected power value to be associated with the point on the side of the gaussian peak from which it originated. This was not the case due to a phase error in the DAQ card producing signals 1 & 2. The phase of these signals was preserved by generating signal 2 from signal 1 directly using Schmidt triggers [3]. This modification offers greater stability than previously achieved when the PC controlling the system generated signal 2.

The second error caused the interrogation system to sporadically fail to locate and lock on to peaks in the reflected spectrum. This was due in part to the algorithm that located the peaks from the initial course scan of the entire spectrum. This algorithm has now been rewritten and this effect has been drastically reduced. However a intermittent problem with the reliability of the lockin process is still observed resulting in the system locking onto and monitoring the next grating in the spectrum.

A number of software changes have also been completed to enable the system to be used to measure static strains accurately (using repeated averaging) and to enable the sampling speed to be increased to facilitate the observation of strain transients during impact. A maximum sampling frequency of 200Hz was achieved.

3.4 Summary of Alternative Interrogation System Development

The lion share of the research effort to date on this project has been directed towards the creation of an alternative interrogation technology. The systems under development will if realised enable very high accuracy strain resolution using TDM. However due to the method by which the centre wavelength reflected by each grating is determined and the agility of the system WDM may also be possible using this configuration. Whilst this work has concentrated on one possible method of interrogation much of the work could be transferred to, or would be useful in the development of, alternative interrogation systems.

The new system has some similarities with the previous TDM system in that it utilises an Acoustic-optic Tuneable Filter (AOTF) to select particular wavelengths in the reflected spectrum. Similarly the system can be software controlled via a PC with suitable I/O datacard capability. However, the new interrogation system dispenses with the electronic feedback control to lock onto the centre wavelength of each grating. Instead a number of strategic points on the spectrum are selected and repeatedly scanned and these values logged. An algorithm (proposed by J. Dakin, P. Hill and D. Guerrier) is then used to determine the centre wavelength of each peak (and hence grating) in the reflected optical signal. A super-luminescent source (a short (7m) Erbium doped fibre pumped with a 980nm 10mW laser) replaces an Edge Light Emitting Diode (ELED) as the light source in the system to enhance the optical output and hence reduce the noise in the system. In the last month the system has been successfully modified to utilise a digital frequency synthesiser rather than a Voltage Controlled Oscillator (VCO) to supply the RF drive for the AOTF which improves the purity and stability of this signal.

3.5 Details of Interrogation system development

A number of interrogation system configurations have been evaluated in the course of development of this technology at the University of Southampton. All use the same method of system control in that a PC is used to set the centre wavelength of the optical filter (AOTF) giving it overall control of the external process. This was initially achieved via the analogue output of a National Instruments' (N.I.) PC-MIO-16XE which set the output frequency of a voltage-controlled oscillator or multivibrator. Now the frequency synthesiser is controlled via the digital output port of a N.I. PC-DIO-32HS.

A number of possible methods of producing tuneable narrow-band light using an AOTF already exist. This filter operates by means of the interaction between an acoustic standing wave and a light beam travelling through a tellurium oxide crystal. The advantage of this method of optical filtering is that, merely by changing the frequency of a RF drive signal producing the acoustic signal, the centre wavelength of the filtered light can be altered under electronic control. This allows tuning of a filtered light source to scan through the entire wavelength range (1520-1600nm) covering a complete array of gratings. In all possible configurations of the light sources described below, the basic method of tuning the AOTF was the same. The typical transmission spectrum of the AOTF is shown in Fig. 22.

All configurations use the same sampling and interpretation system which measures the reflected optical power at each selected wavelength with a photodiode connected via a transimpedance amplifier (both found in an integrated component LAD40 by TheoOptics) to the sampling analogue input of the PC-MIO card. The maximum rate at which the PC can perform

analogue I/O is 100kHz. Hence the PC is now used as the basic pre-conditioner, data-gathering element, and data processing and logging unit.

Fibre Bragg grating strain sensor peak wavelengths are calculated by comparison with the output signals (and therefore RF drive frequencies) needed to address known-wavelength reference gratings. The main advantages offered by this configuration are that multiplexing is now performed by means of fast sequential reading of each grating and there is less dedicated electronic hardware to construct. In addition, being under software control, the system becomes ultimately much more flexible in operation. This offers a number of advantages over the TDM system used previously which utilises a dedicated tracking loop to allow the AOTF to track a single grating, whence the mean AOTF frequency was then measured by a counter.

The only difference between each version of the new system is the optical configuration.
Each configuration investigated is detailed below and a short discussion of the associated advantages and shortcomings included. Individual system components are then discussed. At present the fourth configuration presented offers the best performance in terms of output power, line width reduction, and system agility and is currently the favoured option.

3.5.1 Optical system configurations

Filtered broad band source

The initially proposed design for the interrogation system suggested the use of a broadband source (either ELED or rare-earth-doped fibre source) unit, followed by a combination of an AOTF and optical detector to act as the scanned optical spectrum analyser (Fig. 26). Together, these would allow determination of the peak wavelengths reflected by the gratings. Available ELED sources, whilst convenient, are not very powerful devices, delivering only of the order of 100 μW useful power in the fibre over the whole bandwidth. In addition most of this emitted light is then filtered out on passing through the AOTF. This is further compounded by the fact that, even at the peak wavelength of its pass-band the AOTF still has an attenuation of 6dB. This means that for a typical AOTF-filtered ELED source we could expect to obtain useful narrow band light power of the order of 1 μW (approximately 25 to 30 dB attenuation when taking both the loss at peak transmission, and the narrow-band filtering action into account).

The problem of low light level for interrogation can be substantially decreased using a rare-earth-doped fibre light source. Here, instead of using a diode as the broadband light source, a section of Er^{3+}/Al-Doped Fibre Amplifier (EDFA), pumped by a 980nm semiconductor laser, is configured in a super-luminescent configuration. This EDFA generates light by spontaneous emission, which is then amplified substantially by passage along the amplifier fibre. In the absence of any filtering, an Amplified Spontaneous Emission (ASE) broadband source is obtained, the spectrum of which can be seen in Fig. 23. The light levels available from such a source greatly exceed, by typically 2 to 3 orders of magnitude, those, which are available from a 1500nm ELED source. Such a source can typically deliver a broadband output of the order of 5-10mW from a mono-mode amplifier fibre that can then be efficiently spliced or connected to standard fibre of similar core diameter.

Commercially available versions of the desired narrow-band AOTF filters were found to have significant side-lobes, the strongest lobes having only about 12dB less transmission than the peak transmission value of the filter (which can be seen clearly in Fig.22). These could cause significant cross-talk when used to interrogate gratings of closely spaced wavelength. These sidebands, are an intrinsic feature of currently available AOTF devices. It is possible to improve the performance of the AOTF and suppress (spread) the side-bands using signal-processing techniques (e.g., by frequency modulation of the drive signal) but this leads to only relatively modest improvements. If substantial side-band suppression is desired, then other approaches must be used.

Double filtered broad band source.

A variation of the simple system detailed above is to place the AOTF in the fibre lead to and from the grating array (Fig. 27). This has the advantage of filtering the light twice, firstly in the outward direction, and again on its return, after reflection from the gratings. The second filtering further suppresses the AOTF sidebands (doubles the dB losses at the sidelobe wavelengths) and also reduces the effective filter linewidth. The disadvantage is that there would be further loss of power (typically around 7 to 10dB additional loss) due to the additional attenuation due to passing through the AOTF a second time.

Super regenerative source.

The third configuration suggested stems from the realisation that the available light would be increased greatly and sidelobes would be reduced if the AOTF could be included in a regenerative ring containing a rare-earth-doped fibre amplifier. Then, light at the wavelengths corresponding to undesirable side-lobes in the filter would be repetitively attenuated, as a result of repeated passes through the ring, whereas the desired light, at the peak transmitted wavelength would suffer either amplification or negligible loss, depending on the amplifier gain level. This would result in a narrowing of the filter line-width, a suppression of the AOTF sidebands and the concentration of available power into the filtered output spectrum. In the extreme case, if enough of the light were to be allowed to re-circulate to give a loop gain of unity or more, it would result in oscillation, in the form of a tuneable ring-laser system.

Even without lasing, the available intensity of narrow-band light in this type of regenerative loop is much greater than with the previous systems, provided the loop gain is not allowed to be much less than unity. Unfortunately, however, allowing a system to lase can frequently give rise to problems of coherent addition of many tiny reflected signals. Examples of the problems that can occur include coherent backscatter or the coherent addition of multiple Fresnel or even of multiple grating reflections leading to speckle noise (i.e. laser aspeckle effects) and the possibility of the laser locking onto particular wavelengths corresponding to small peaks in reflectance of the sensor array. The latter can cause undesirable "mode-hopping" as the frequency of the tuning element is scanned.

In order to take advantage of the regenerative recirculation method, whilst avoiding undesirable lasing, the ability to electronically control the attenuation of the AOTF can be used to advantage. To achieve this the amount of light re-circulated round the loop containing the EDFA must be carefully controlled to give a loop gain just less than unity. If the loop gain were to be allowed to fall way below unity, very little power would be generated and the line narrowing and side-lobe suppression of the AOTF filter characteristics would not occur to such an extent, i.e. the system would not operate with maximum efficiency.

Control of the system is not easy, as the spectral gain curve of the EDFA is not flat across the bandwidth of interest. Particular care must therefore be taken to prevent lasing occurring at certain wavelengths where the gain is particularly high. In an attempt to control this, a proportional feedback controller was constructed which modulated the RF drive signal to the AOTF. Since there is a convenient region where the transmission of the AOTF is roughly linearly proportional to the RF drive level (see Fig 24), this offered an ideal method of controlling the light level within the loop. This was further simplified by the fact that our AOTF driver had an Active Gain Control (AGC) input, allowing control of its RF gain by using a low-voltage control signal, in the 0 to 5-Volt range.

Further modification of the basic loop was carried out by introducing a 90% : 10% coupler after the AOTF to usefully remove 90% of the light from loop directly after passage through the AOTF (see Fig. 28.). The in-loop attenuation provided by this coupler meant that the AOTF was generally operated at a setting with relatively high transmission. Otherwise, without it, it was necessary to attenuate heavily in the AOTF to keep the loop gain below unity. The arrangement in Fig. 28 provided a non-lasing, narrowband light source, of typically 0.5nm bandwidth, which was tuneable over the range between 1520 and 1560nm wavelength, and provided an optical power of typically 40μW in the desired narrow band. This source gave around 30 to 40dB greater power in the desired narrow band than was available from an AOTF-filtered ELED system.

Fig. 25 shows a typical narrow-band optical spectrum for such a source when using a relatively modest (120mA) drive current to the 980nm pump laser. It is clear that there is of the order of

20dB side band suppression, compared to that of only 10dBfor a single pass configuration for the same AOTF (Fig. 22). The limits of side-band suppression depend only on how closely the system can be controlled to give unity loop gain, without undesirable lasing, so there is still scope for further improvement.

After continued investigation it became clear that the addition of the optical loop gain control unit significantly reduced the sampling rate of the system (to as little as 2kHz). Attempts to increase the agility of this unit resulted in an increase in noise in the optical system and uncontrolled lasing at wavelengths corresponding to the regions of highest fibre amplifier gain. However the replacement of the VCO (analogue control) with the digital frequency synthesiser (digital control) has freed an analogue output from the PCI-MIO card. It is possible that this output could be used to control the loop gain of this configuration. After calibration has occurred this output could set the AGC voltage using a look up table with values set for each corresponding wavelength scanned. At present this option has not yet been investigated, as a more practical optical configuration is possible.

Double pass tuneable source

This configuration enables a narrowing of the filter line-width, suppression of the AOTF sidebands and the concentration of available power into the filtered output spectrum. Fig 29 illustrates this configuration. A single 980nm-pump laser is used to pump two lengths of Erbium Doped Fibre. The first length has no incident light in the 1520 - 1600nm window and hence acts as a superluminescant source. The efficiency of this source is enhanced by front end pumping and mirroring the free end to return the light that would otherwise be lost (both 980nm and 1520 - 1600nm). The second length of Erbium Doped Fibre is used as an Erbium Doped Fibre Amplifier (EDFA) as emission at the output wavelength of the source is stimulated by the incidence of filtered light from the superluminescant source via the AOTF. The use of a circulator and the addition of a mirror on the free end of this EDFA allows this amplified light to return through the EDFA and the AOTF. This reduces the line-width, suppresses the side-bands, concentrates the power into the filtered output spectrum and increasing the available power in the output of this tuneable source. The addition of this mirror also has the consequence of reflecting any unabsorbed 980nm pump light back into the EDFA for a second attempt at powering the stimulated emission of light.

Although the super-regenerative loop when operating efficiently can offer better performance for all these effects this configuration still offers a number of advantages. Firstly there is no requirement for control of the AOTF transmission loss as a function of wavelength to the same degree of accuracy as the lasing condition is not possible. It may be possible to do without an AGC unit altogether as spectrum flattening can be achieved by other means. The removal of the AGC unit greatly increases the sampling rate possible; indeed with the use of a frequency synthesiser (rather than a VCO) the data acquisition card now imposes the fundamental limit on the system sampling rate (100kHz). If the spectrum of the source were to need modification several options are still open.

- Utilise the spare analogue output from the data acquisition card to control the AOTF transmission.
- Place passive optical filters on the output of the tuneable source
- Taylor the reflectivity spectrum of the mirrors employed (either by the use of filters or replacement of the mirrors with gratings with reflection characteristics tailored to the required output spectrum).
- Flatten the gain of the tuneable source by varying the length and doping levels of the erbium doped fibre and by carefully controlling the 980nm laser pump power for both the superluminescant source and the Erbium Doped Fibre Amplifier (EDFA).

At the time of writing this configuration is not fully implemented. However, part of this configuration has been tested by constructing the system without the EDFA between the AOTF and the mirror connected directly to it and without the mirroring on the end of the superluminescant source.

3.5.2 System Components

The following system components listed are common to all the optical system configurations with the exception of the feedback system to control regenerative loop gain in the super regenerative source configuration.

Feedback System to control regenerative loop gain in Super regenerative source configuration

It is necessary to have a feedback system to control gain to prevent oscillation (lasing) in the regenerative loop containing the fibre amplifier and the AOTF. The use of an intensity control method also has the added advantage of greatly decreasing the wavelength-dependent fluctuations in the EDFA output, which can otherwise lead to wavelength errors.

Fig. 30 shows the two-stage circuit constructed for this purpose. The first stage consisted of a PIN diode detector in a DC-coupled transimpedance receiver configuration. This gave a voltage output level proportional to the intensity of a controlled fraction of light from that re-circulated through the loop, this fraction being selected using the 9:1 fibre coupler. The second stage of the controller was a simple band-limited inverting amplifier stage, which fed a control signal to the AOTF driver. This was relatively simple to arrange, because the RF amplifier used to drive the AOTF was fitted with a control port. Application of a zero volt DC signal prevented any RF transmission through the amplifier and positive voltages gave increasing gain, until a voltage of 5V gave maximum gain. As the input optical power rises, the output voltage falls proportionally, decreasing the gain of the RF driver and consequently acting to increase the attenuation of the AOTF (see Fig. 24), thereby controlling the light level in the loop.

Some initial problems with the stability of the control loop were experienced. There was one particular resonance that occurred in the loop at a frequency of approximately 16kHz that caused a lot of problems. The solution to this was to introduce an element of phase lag compensation (further band limiting) into the control circuit. This took the form of adding a 2.2nF polystyrene capacitor in parallel with the feedback resistor of the transimpedance amplifier. The problem with this solution was that it was necessary to reduce the upper 3dB point of the control circuit to around 2kHz to maintain stability. Although workable in a slow measurement system, this was felt to be undesirably slow and other methods, namely phase- lead control, were then investigated in an attempt to increase the bandwidth of this controller. However a solution was not forthcoming and hence this unit is not employed in the current configuration.

RF generation unit, for computer-controlled generation of the RF drive signal to the AOTF (common to all configurations)

As described above, the AOTF filters light by means of a polarisation-dependent interaction in a transparent TeO_2 crystal, driven acoustically by a piezoelectric transducer, which is itself energised using a RF drive signal. In order to provide optical tuning over the desired gain band of the Er fibre amplifier (1520-1560nm), the acoustic frequency required from the piezoelectric transducer is in the region of 82 to 87 MHz. Initially a high-slew-rate, voltage-controlled oscillator (VCO) was used but was later replaced by a digital frequency synthesiser to improve the performance of the RF generation circuit.

A sufficiently agile RF generation unit allows the frequency of the generated RF signal to be rapidly varied, thereby tuning the AOTF quickly across the optical band of interest. The AOTF itself can be tuned to a new frequency in around 10 microseconds, so the limitation is set mainly by the slew-rate capability of the RF generation circuit.

<u>VCO</u>

Initially the AOTF RF drive signal was produced by a high-slew-rate, voltage-controlled oscillator (VCO). The voltage used to tune the VCO was derived from a multi-channel input/output card within the PC, where a digital signal was converted using a 0-10V DAC chip with a 16 bit accuracy. Fig. 31 shows the circuit for the VCO. In order to obtain the maximum VCO-setting resolution over the desired tuning range, the 0-10V output had to be scaled using an input stage. This consists of a differential amplifier, to subtract the 0-10V DC input from the PC output port from a precision reference-voltage source, and multiply the result by a factor set by a control

potentiometer. The output signal from this first scaling stage was then fed to the control pin of a voltage-controlled multivibrator chip (Motorola, type MC1658) the square-wave output of which was buffered with Emitter-Coupled Logic (ECL) gates. All the critical components in the VCO unit were mounted in good thermal contact with the box containing it, so that all frequency-controlling elements within the unit could be more easily temperature controlled.
To verify and calibrate the actual tuning of the VCO input stage a digital voltmeter (DVM) was used to check the input signal (i.e. the o/p from the PC card) and a precision frequency counter was attached to the VCO output. This provided a convenient and accurate means of setting the desired RF output frequency range. The VCO tuning curves, as a function of housing temperature, are shown in Fig. 32, for three different settings of the temperature controller. It can be seen that the linearity is excellent, but there is a strong dependence on temperature.

A further concern regarding the VCO was whether the internal chip temperature showed any variation with switching frequency, as ECL chips are known to generate significant heat. In order to investigate this, the VCO frequency was measured at a selected drive voltage, V_o, to give an output frequency, F_o. Then, the drive voltage was held to give a frequency above F_o for a short interval, and then returned to V_o. It was found that the frequency took a short interval, of the order of 0.5 seconds to return to the expected steady-state value, F_o. A similar but inverse behaviour was observed if the frequency was altered in the reverse direction.

At first it was thought that this behaviour would not be of serious consequence if it were fully reproducible, or if the system were scanned too rapidly for significant temperature differences to arise during the duration of the scan. In addition it was envisaged that further compensation could be provided by a software change to measure the system in both ascending and descending frequency sweeps and averaging over equal numbers of each. This software was constructed but offered no improvement in the high levels of noise observed in the system.

Examination of the VCO output on a RF spectrum analyser and with a high-speed frequency discriminator revealed that this component was responsible for the addition of considerable levels of noise in the system. The output had noise components at both low and high frequencies and in addition the output level was poor and exhibited a high level of erratic phase noise. In addition the rise time of this unit was significant in the total settling time of system and despite modifications to both the conditioning circuits and replacement of the multivibrator chip with alternative units these problems persisted. At this stage the risks of continuing with this method of RF generation were perceived to be higher than other methods. Therefore, research in this area has been terminated.

Frequency synthesiser as replacement for the VCO

Frequency synthesisers are attractive as replacements for the VCO as RF frequency sources due to the high rates of frequency modulation (50MHz+), modest output power, and high output stability (mHz) possible. Two frequency synthesisers (AD9832 and AD9850) have been evaluated in the lab whilst a third (AD9852) has been considered from the information available from its documented technical specifications. All three devices are produced by Analog Devices Inc. and require high speed digital I/O to set a new RF output at the required modulation frequency (100kHz). This can not be achieved with the PC-MIO-16XE data acquisition card. hence a PCI-DIO-32HS has been integrated into the system to perform the digital I/O functions.

The AD9852 is the only device that produces a fundamental output in the desired frequency range (82 - 87MHz) directly but at the time of writing is not commercially available. However the provisional technical specifications [4] indicate that this component is more than capable of reaching all the requirements for this system and could be tried at a later date.

The AD9832 is limited in fundamental output to 12.5 MHz. Therefore use of this device would necessitate the generation and filtration of harmonics to produce a signal of the required frequency. This would require times nine frequency multiplication which although technically feasible presents a number of practical problems in the creation of a unit capable of this task. In addition the programming of this unit is via a serial port only which increases the demands placed on the digital I/O card in the PC. This would either necessitate the creation of additional digital I/O buffer hardware or the reduction in the modulation frequency of the RF signal thus reducing the sampling speed of the system as a whole.

Although the AD9850 [5] does not produce a fundamental in the required frequency range its higher frequency output (<33Mhz) and clock frequency (100MHz) enable the creation of a signal in the required range with greater ease than with the AD9832. Three methods of signal creation are possible with this device, all of which have been evaluated in the lab.

Firstly the CMOS output from this device (which should be a square wave with a frequency equal to that of the fundamental sine wave output) will generate a number of harmonics which could be filtered directly to select a signal in the desired range. The third harmonic would be capable of producing the desired tuneable signal. However the CMOS output from this device is not a pure square wave and hence a number of subharmonics and reflected signals prevent this method producing a signal of the required purity and stability.

Frequency multiplication of a factor of three can also be achieved by the combination of two mixer units. Mixing the fundamental with itself produces the second harmonic. If this second harmonic is then mixed with the fundamental the third harmonic is produced. A unit for this purpose was realised in hardware but failed to produce a signal of the required stability or purity due to a high sensitivity to nonlinearities in the hardware and impurities in the fundamental signal.

Finally it is a characteristic of sampling based frequency synthesisers that a signal is found in the unfiltered output of the device that is of a frequency equal to the clock frequency minus the fundamental frequency. This effect is expected from the Nyquist sampling theorem [6] and can be used to advantage for this application. If the fundamental is set such as to produce this alias signal in the required frequency range it then remains to separate this signal from the fundamental and the clock frequency which are both present in the sine wave output of this device. This was achieved by the use of a 100MHz high pass filter (to remove the fundamental), a 100MHz notch filter (to remove the clock frequency) and a suitable band pass filter and amplification unit to boost the power of the required signal. This arrangement has now been realised in hardware. The frequency response of this signal processing unit and its components can be seen in figures(34-38). Figures (39 & 40) show the spectrum produced by the RF generation system at a typical output frequency which can be compared to fig 41 which shows the frequency synthesisers output spectrum. It can be seen that after filtration and amplification the desired signal dominates the spectrum (45dB in band, 15dB out of band) in the required range, hence this unit has now been integrated into the system and has been shown to allow accurate stable and low noise tuning of the AOTF.

The inclusion of a frequency synthesiser has a number of advantages. Of particular benefit is the high tuning speed now feasible. In this instance the tuning speed of the AD9850 is limited by the output speed of the digital I/O transfer which is dictated by the PC card. However RF modulation is now possible at 1MHz hence the RF generation circuit no longer limits the speed of the system as a whole.

Optical detection system for monitoring power reflected from the grating array (all configurations)

The detector used for the return power measurements from the array is an LAD40 device from TheoOptics and provides a reliable measurement of the light level reflected from the gratings for a given input light signal.

Temperature stabilisation of key components (all configurations)

Initially the temperature stabilisation was achieved by circulation of water (flow rate of approximately 10 l/min) from a commercial temperature-controlled (0.1C - accuracy) bath. This water circulation circuit contained a number of specially made heat exchange elements, which could be placed in thermal contact with the components to be temperature controlled. Of the elements in the system, the most temperature-critical are the AOTF, the frequency synthesiser reference clock and the DAC and ADC chips on the PC interface card. The intention was to run the temperature-controlled bath slightly above ambient temperature, to prevent condensation within any of the elements. However this stabilisation system was initially created in an attempt to stabilise the VCO which exhibited properties that were extremely sensitive to temperature. Now that this unit has been replaced there is less need

for such a system and it is expected that the remaining thermal effects will not be significant for the measurement of impact induced strain.

Of the remaining components the reference gratings are the most critical in terms of thermal control, as they are used as calibrators to check for residual drift, after all our other design measures have been included. For this purpose a precision temperature controller was constructed. This utilises a thermistor bridge, to control the temperature of an aluminium cylinder, which houses a thin-walled, glass-capillary tube (which provides strain isolation), in which reference gratings can be inserted (Fig. 42). These gratings will then act as precision calibration points for the system, allowing compensation for any residual drift, etc, of the interrogation system to be applied to the measurements. This temperature-controlled housing has been tested and found to control the aluminium cylinder housing the thin capillary tube to approximately +/- 1 mC.

3.5.3 Interrogation algorithm and software

The system has been designed so the majority of the signal processing and system pre-setting and control can be carried out in the software. The computer controls the frequency of the tuneable source by outputting signals to the frequency synthesiser driver board, and receives and processes the resulting return signal from the sensor array. The system is operated in two modes, firstly an initial set-up mode that operates by slowly monitoring the reflection spectrum of the array and determines the characteristics of each sensor element, and, secondly, a reduced-data mode that determines selected wavelength-critical parameters of each grating (effectively the wavelength of the rising and falling edge positions of each grating reflection) in a repetitive fast-scan mode.
The basic method of operation of the system program is detailed in Appendix 2.

The software was developed using one National Instruments (NI) product, called Lab-Windows CVI (meaning C programming for Virtual Instruments) and another called NIDAQ (National Instruments Data Acquisition). When used with two National Instruments, input/output (I/O) boards for the PC (analogue and digital, type number PCI-MIO-16XE-10 and PCI-DIO-32HS) these allowed the programmer to write, develop and debug system operating code for the project. It also allowed integration of a Graphical User Interface (GUI), allowing the program to interact with the user.

3.5.4 System Resolution

The accuracy of the interrogation method is dependent on many factors, including the noise in the optoelectronic system, the stability and purity of the RF signal, the accuracy of the input voltage measurements and the reliability of the calibration & correction procedure. Apart from the accuracy of the calibration experiments, the latter will depend on the reproducibility and linearity of the overall measurement system.

The control of the frequency synthesiser uses a 32 bit tuning word which controls the output frequency linearly from 0-100% of the clock frequency. The alias signal is controllable with the same resolution as this is equal to the clock frequency minus the frequency of the fundamental. Therefore, the output of the RF generation circuit is controllable to 0.023Hz (although its stability is less). If the system were noiseless this would allow control of the AOTF centre wavelength to 0.4fm. Even if the system were noiseless it would be impractical to scan across the optical window at this resolution as the data set generated would be extremely large and unwieldy and would require more processing power than available in a standard PC. It is also well understood that the system is not noiseless and that even if this huge data set were to be recorded the location of peak power (reflected by a greating) would not be at the absolute local maxima in returned optical power. If this method were to be used to locate the centre wavelength of each grating the result returned would be too dependant on noise in the system. Hence a more sophisticate algorithm for grating wavelength determination has been developed. This algorithm is described in Appendix 2.

A further method of increasing the resolution to which the reflected intensities can be read was proposed, as this used an A/D converter with only 16 bits. This method consisted of calculating a voltage reference level for each grating in the software. This reference level would be set to be slightly below the level of the lowest-measured signal voltage likely for a given grating. The actual voltage measured by the PC would then be measured from the optical receiver output relative to this reference voltage level via a differential amplifier.

The method effectively involves subtraction of the pre-set reference voltage from the output from the optical receiver, so that the 16-bit readout is performed over a narrower voltage range. Provided the reference voltage subtracted is stable and constant during all the measurements on a single grating peak, it would not need to be known accurately, as the interrogation algorithm then subtracts readings taken on the rising and falling edges of each peak. On passing to measure each of the other grating reflection peaks, this subtraction voltage could be adjusted to a new level if desired; to correspond to a different reflected intensity level for each peak.

Whereas future provision has been made for this facility in both the hardware and the software, it has not been implemented, as it is expected that system noise will normally preclude the need for it.

3.5.5 System speed and WDM

For a discrete sampling interrogation system the maximum frequency at which dynamic strain can be resolved is given by equation 1:

$$f_\varepsilon = \frac{f_s}{n_g n_p n_s n_a}$$

Equation 1.

f_ε = maximum dynamic strain resolution
f_s = sampling frequency
n_g = number of gratings
n_p = number of points per grating required to enable peak determination
n_s = number of samples per cycle required to enable resolution of dynamic strain waveform
n_a = number of iterations to improve the signal to noise ratio by averaging

The maximum possible sampling rate with the above system is currently 400Hz (f_s = 100kHz, n_g = 4, n_p = 6, n_s = 10, n_a = 1) but significant improvements could be made. For example n_p could be reduced to four with minor software alterations or to two if the slopes on a grating peak were to be evaluated before a data-logging run were started. n_s could be reduced to 5 if less detailed information about the shape of the waveform were required. These improvements would allow a sampling rate up to 2.5kHz for four gratings given that no averaging was required to improve the signal to noise ratio.

If the dynamic strain resolution cannot be improved then spare capacity in terms of system speed can be used to take multiple readings of any residual strains and hence improve the signal to noise ratio / resolution of the TDM sensor.

4 Conclusion

Bragg grating strain sensors have been shown to be capable of providing distributed strain sensing for CFRP laminates that can enable in situ and in-service health monitoring. The interrogation technology developed by H.Gieger [2] has been successfully adapted for use for impact damage assessment. Despite its relatively low sampling rate both dynamic and

residual strain information can be ascertained for a given impact. Dynamic and residual strain information has been shown to vary with material properties and with relative impact location.

High-speed digital photography has given a valuable insight into the response of materials to impact damage and allows the sensor readings gained to be placed in context. This is a useful and powerful tool for impact experimentation.

Significant steps have also been taken to improve interrogation technology. These improvements will allow an increase in the resolution of optical bragg grating based sensor arrays. However it has been demonstrated that the existing technology is capable of measuring and characterising impact damage as required.

5 References

1. Taylor E A, Herbert M K, et. al. Hypervelocity impact on spacecraft carbon fibre reinforced plastic / aluminium honeycomb. Journal of Aerospace Engineering, No G5, Vol. 211, 1997. ISSN 0954-4100

2. Geiger H. Quasi-Distributed Optical Fibre Strain Sensors. PhD Thesis, University of Southampton, April 1995. P 110-142.

3. Trundle K.J. Temperature and strain cross sensitivity in fibre Bragg grating sensors. Internal Report, Optical Fibre Group, Sept Electronics and Computer Science Southampton University.

4. AD9852 Component Data sheet, Analog Devices Inc., see: http://products.analog.com/products/info.asp?product=AD9852

5. AD9850 Component Data sheet, Analog Devices Inc., see: http://products.analog.com/products/info.asp?product=AD9850

6. AD9850 Component Data sheet, Analog Devices Inc.,(pg.7), see: http://products.analog.com/products/info.asp?product=AD9850

Appendix 2. Software Methodology

A sequential description of the algorithm used to calculate peak wavelength from reflected spectral data is listed below.

1. Perform initial scan of reflective spectrum from grating array, at all wavelengths between pre-set endpoints. The purpose of this scan was to provide an overview of the shape and position of all the grating reflectivity peaks. This is an essential initial part of the set-up procedure, which, if desired, can be programmed to repeat periodically to correct for any major drift errors. In order to reduce noise in this initial measurement, the initial scan can be repeated a pre-selectable number of times and the gathered data averaged. This initial stage is completed at a relatively low resolution (approximately 0.02nm between each sample point) to increase the speed of the process and to prevent overloading of the processor. This coarse data enables the location of the peaks to be estimated. The exact location of the peak can then be determined by a reduced data scan as described below.

2. Perform moving average filtering of the data from step (a) above. This is necessary to reduce the possibility of noise on the data giving errors in the grating-peak locations

3. Locate peaks of each grating in the reflective spectrum. This provides important starting information for the tracking algorithm. The number of peaks expected is already known (corresponding, of course, to one peak per grating) so it is simply a matter of assigning an initial estimate of wavelength to correspond to each measured grating reflectivity peak. Our positioning algorithm then operates by monitoring, and looking at the changes in, the slope of the peaks. A change from a positive slope to a negative slope indicates a grating peak. Since the data is real (i.e. measured) data, with inevitably some noise, too simple an algorithm would lead to errors on the peak location. This was avoided by calculating the slope from three points (two pairs of points) some distance apart. When both pairs indicate a falling slope and the central point is beyond the local maximum. The algorithm then sets the peak centre to the wavelength at which the absolute maximum occurred and steps to begin searching the next peak. In order to evaluate the width of each grating reflectivity peak, the position of the minima either side of the reflected peak is found. The minima with the highest reflected power is then used to calculate the reflected power corresponding to half the sum of this and the peak reflected power. This value is the half-height power. The points either side of each peak that reflect power at this value are then located and the grating width is the difference between their locations in the wavelength domian. If sufficient a sufficiently large data set were gathered these algorithms could locate the grating peaks and identify their centre wavelength with sufficient accuracy. However, this quantity of data could not be collected or processed fast enough to allow WDM. Hence the deviations in magnitude of return signals from specified wavelengths on the slopes of the grating peaks are used in conjunction with the measured value of the gradient to measure the strain faster and more accurately. This method can locate a grating peak with as little as four data points or two if the peak slope gradients remain constant and can be determined before a data logging cycle. The following steps describe the enactment of this interrogation method

4. Select near-half-height points. A number of other points in the region of the two half height points are then selected just a few wavelength intervals removed (both in a positive and negative λ direction) from the original half-height points. We shall call these the near-half-height points (See Fig. 33). These are used to reduce possible noise errors that might arise if measurements were taken at just a single point on each edge of the reflectivity peaks. The number and the spacing of these extra points are pre-selectable parameters, and visual markers on the PC display depict these operating points. In addition these points can be dithered in wavelength to collect data from a larger selection of the possible data points. This can be used to reduce the effect of systematic wavelength dependent noise, which would not be achieved by repetition, and averaging of repeated measurements at the same wavelength. The number of dither points and the distance between them can be selected on the graphical user interface.

5. Repeatedly measure reflected signal intensities at the dithered near-half-height-point wavelengths. The digital output of the PC is set to output a series of control words to the

frequency synthesiser corresponding to a set of wavelengths close to the half-height points of a selected grating peak (Initially, these values are selected using information about the edge positions derived from the coarse-scan, set-up run). Simultaneously, a measurement is taken of the corresponding reflected light intensity from the array at these selected wavelengths, in the form of a proportional signal voltage from the detector. Thus, a revised value for the return signal levels, at each of the near-half-height points, is measured, for each grating in succession. This measurement step is repeated a number of times over wavelengths covering the whole grating array. The results of these measurements can be averaged to reduce noise (residual strain measurement) or used individually to track dynamic strain in each grating.

6. Calculation of grating-peak edge slopes. These slopes are calculated from the signal amplitude and wavelength co-ordinates of selected points on the rising (or falling) slopes of the grating peaks. This can be derived from either the initial slow scan or from a number of near-half-height point measurements. The signal/noise can be enhanced by averaging the slope between several pairs of closely spaced points on each rising and falling edge of the grating peak. It is important that the slope of both the rising and falling edges of each peak is measured and calculated separately, in case of any asymmetry. A simple linearity check can be carried out at this stage, by comparing the value of the slope with the previously calculated value (or, if this is the first cycle of the fast-scan algorithm, the value calculated at the near-half-height-point amplitudes from the initial spectral scan). If the difference between these slopes is greater than a certain predetermined value, it is considered that the grating peak is too far of centre, and that the half-height points are not yet in the approximately linear region of the grating peak sides. Under such conditions, the value of any calculation of the wavelength for that particular peak would be unreliable. An error flag is set to indicate this condition, which is only expected during early stages of lock-in, or if a sudden transient shock (e.g., sudden pressure front) were to influence the array.

7. Calculation of incremental wavelength shifts of the gratings. An estimate of the magnitude of shifts in the centre wavelength of each grating peak from the initially expected value is now made. This shift then provides a tiny correction, which is added to the wavelength values set by the computer to give a measured real-time wavelength value. The shift of each grating is determined, in turn, from the mean difference in value between sets of reflected signal amplitudes at excitation wavelength values corresponding to sets of points situated on opposite sides of each grating peak. These differences in return-signal amplitudes from opposite edges of the grating peak are divided by the previously calculated value of the mean edge slopes (The mean edge slope is half the sum of the rising-edge slope and falling-edge slope). The values can be averaged over several scans to give an estimate of the overall shift in the grating peak. On the first fast scan, the initial edge-wavelength estimates are determined from the value of the wavelength predicted from the initial slow scan. On subsequent fast scans, these shift values are used to slowly correct the selected edge-wavelength positions (via the pre-set control words to the frequency synthesiser) such that the system follows (I.e. tracks) any large shifts in the grating peak. The advantage of this method is that it reduces the data set required for peak determination. In addition to the real-time settings, all the shift values, representing off-centre displacements of the peak position, are displayed on the GUI. These shift values must be kept small to avoid errors that would otherwise occur due to uncertainties in the precise slope of the edges of the grating spectra.

8. Data logging. The calculation of the wavelength shifts generates a single value of the wavelength shift for each grating every time period. (The duration and repetition rate of this time period is determined by both the sample rate and the number of points to be gathered and averaged.) The format for data logging is to append each measured value for the wavelength shift to the end of the data-logging file. Each file will therefore contain a record of the wavelength shifts for each grating in the form of a matrix where there is a column for each grating and a row for each measurement of the shift at a given time.

9. Preservation of calibration. In order to achieve high accuracy with several thermally-dependent elements in the interrogation system (particularly the AOTF, fibre source and pump laser, and computer I/O, A/D's and D/A's), it was necessary to be able to measure accurately the location of each peak relative to any reference gratings used. In principle, this allowed calculation of the absolute value of the grating wavelengths, and consequently the

strain, through the use of a reference grating of known wavelength kept at constant temperature and strain. It is more likely in practice, however, that a combination of temperature control of critical elements and comparison with a reference grating in an even more carefully controlled environment will be used to render the system stable and reproducible. Then, accurate pressure and temperature values may be obtained after careful system calibration with the sensor array in thermally controlled and hydrostatic-pressure chambers.

Appendix 1 figures

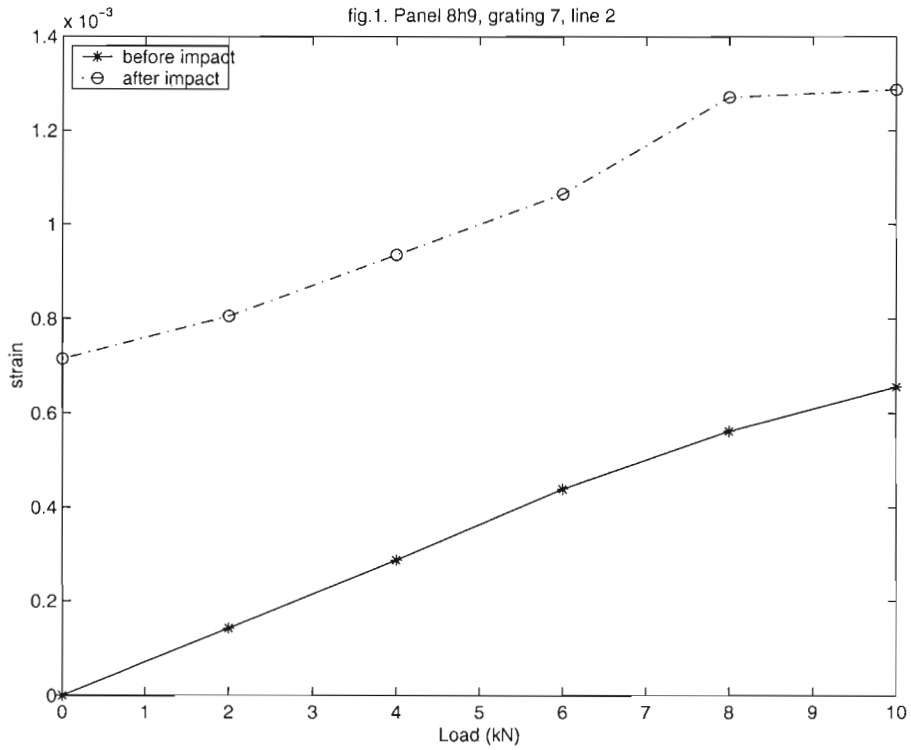

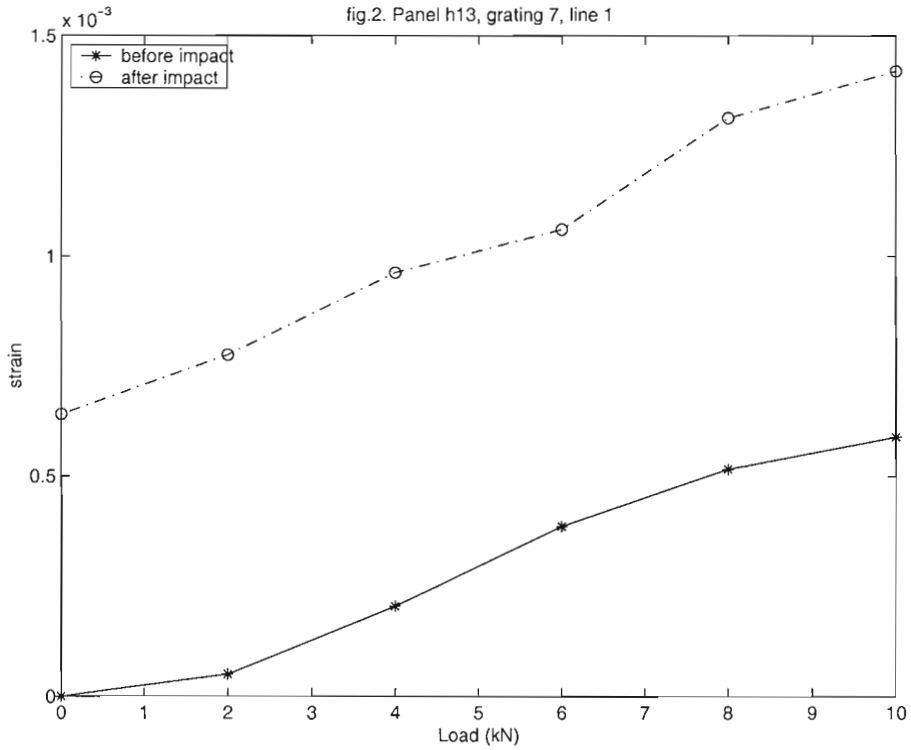

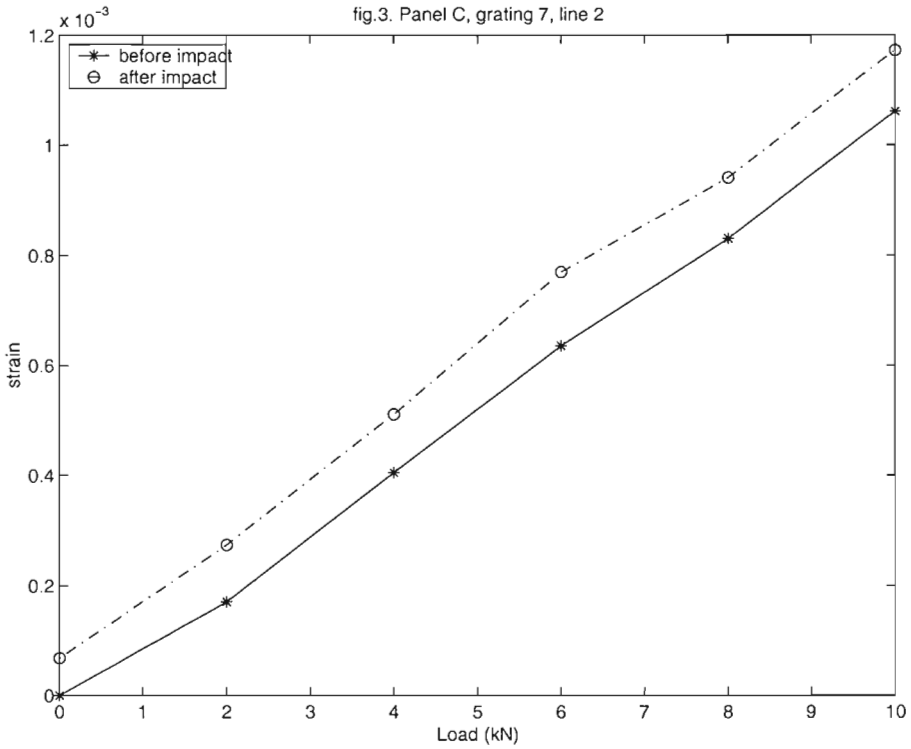

fig 4. Post impact residual strain as a function of sensor location. Panel 8h13.

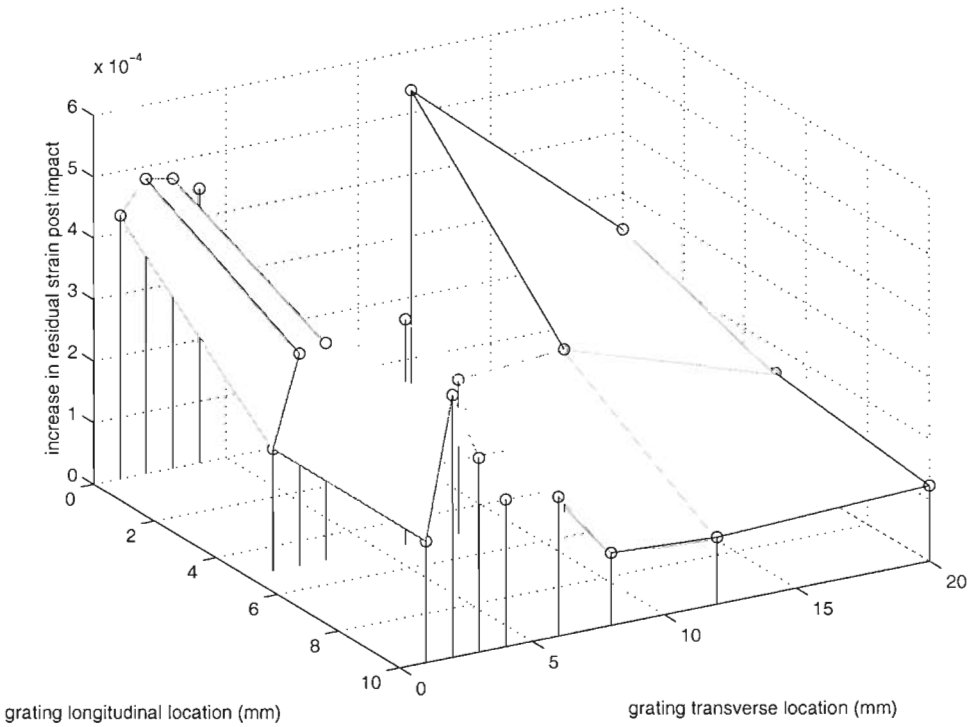

fig 5. Post impact residual strain as a function of sensor location. Panel C.

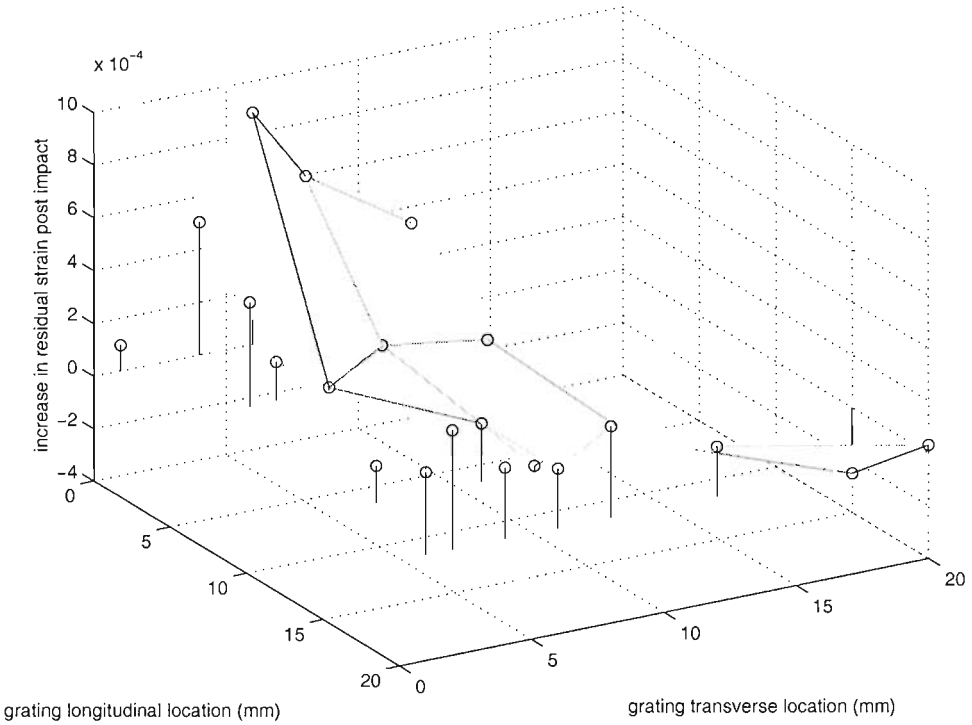

fig 6. Panel 8h13 grating 8 line 1 during impact

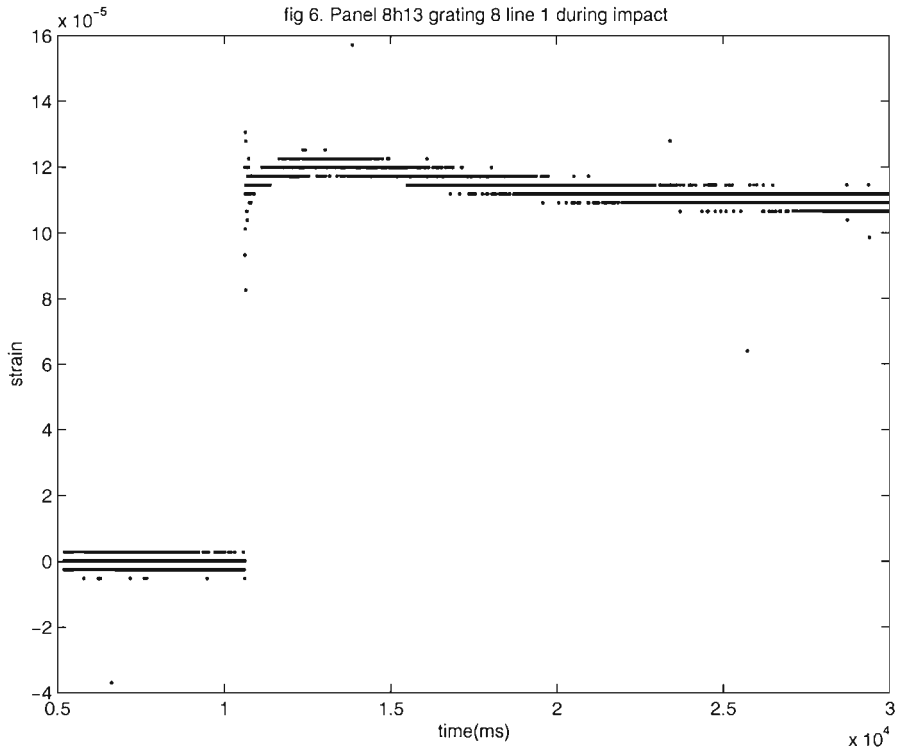

Fig 7 time = 0μs

Fig 8 time = 25μs

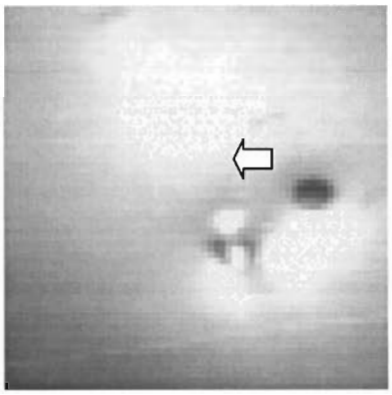

Fig 9 time = 49μs

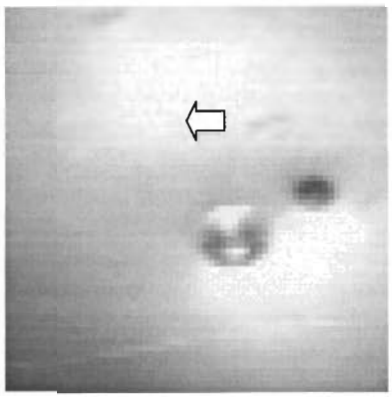

Fig 10 time = 74μs

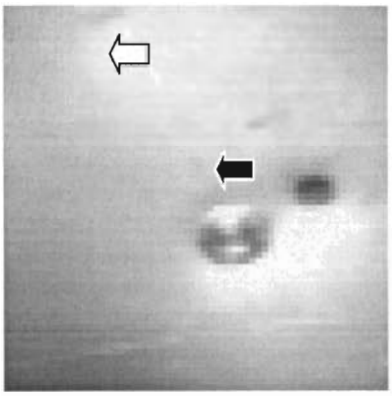

Fig 11 time = 99μs

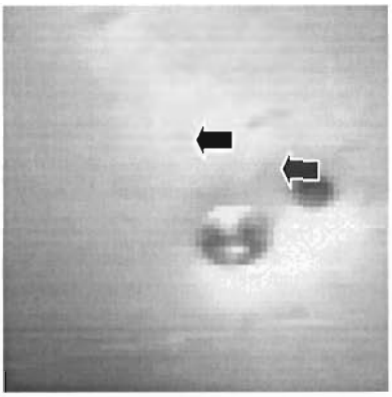

Fig 12 time = 123μs

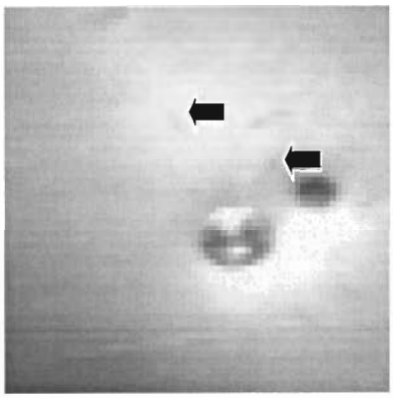

Fig 13 time = 148μs

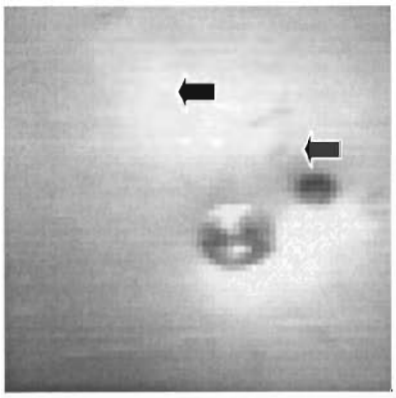

Fig 14 time = 172μs

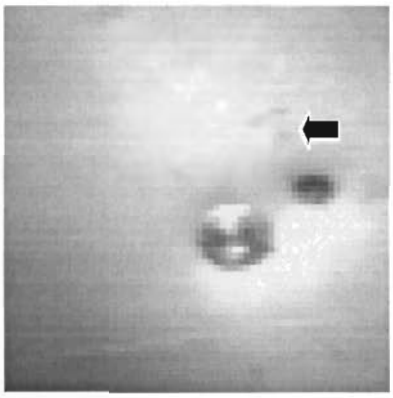

Fig 16 t = 0.47ms

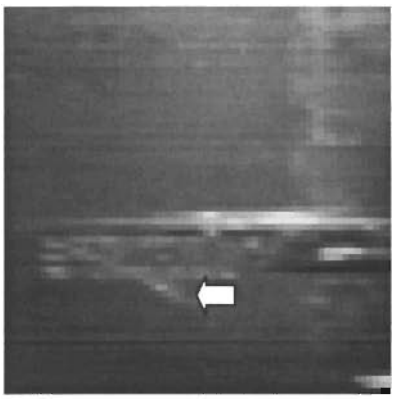

Fig 17 t = 1.28ms

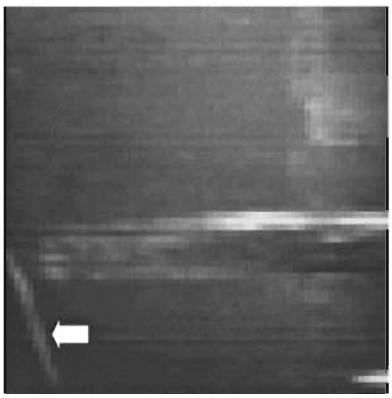

Fig 18 t = 2.27ms

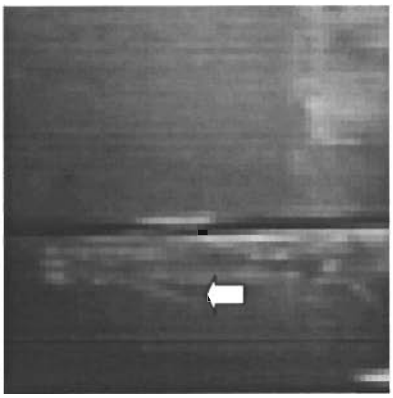

Fig 19 t = 5.36ms

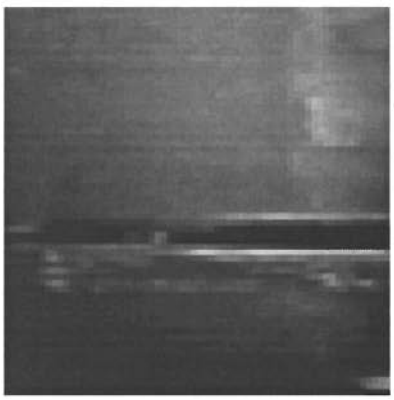

Fig 20 t = 5.70ms

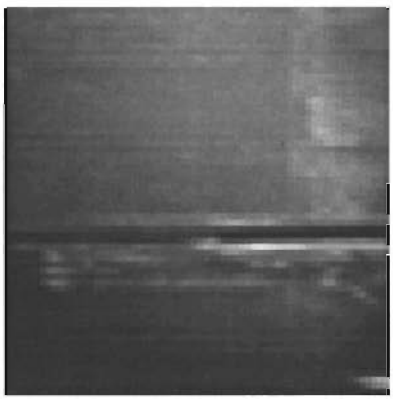

Fig 21 t = 6.25ms

Fig. 22 AOTF transmission spectrum

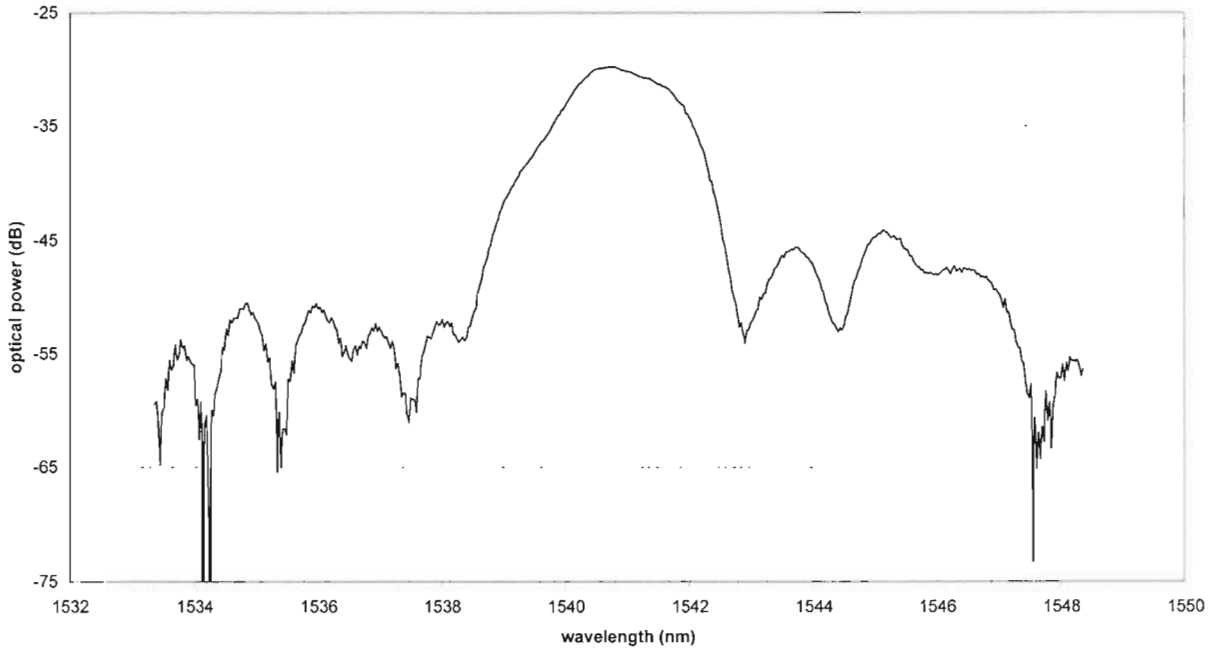

Fig. 23 ASE spectrum

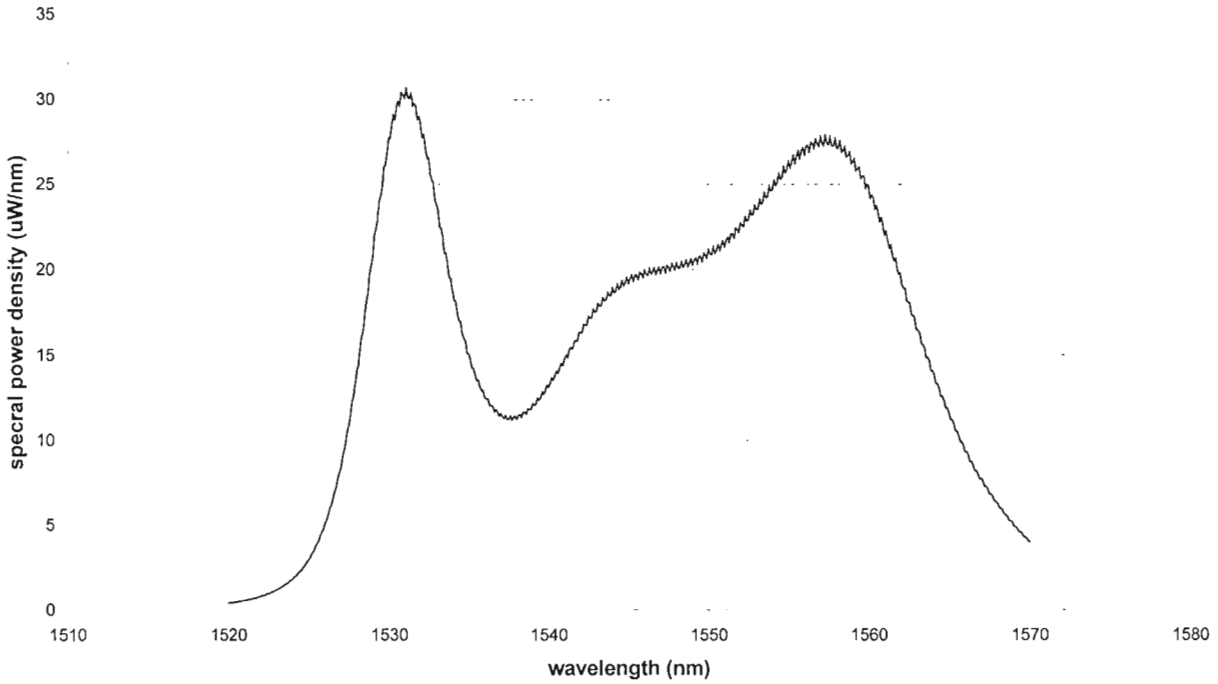

Figure 24. AOTF transmission surface

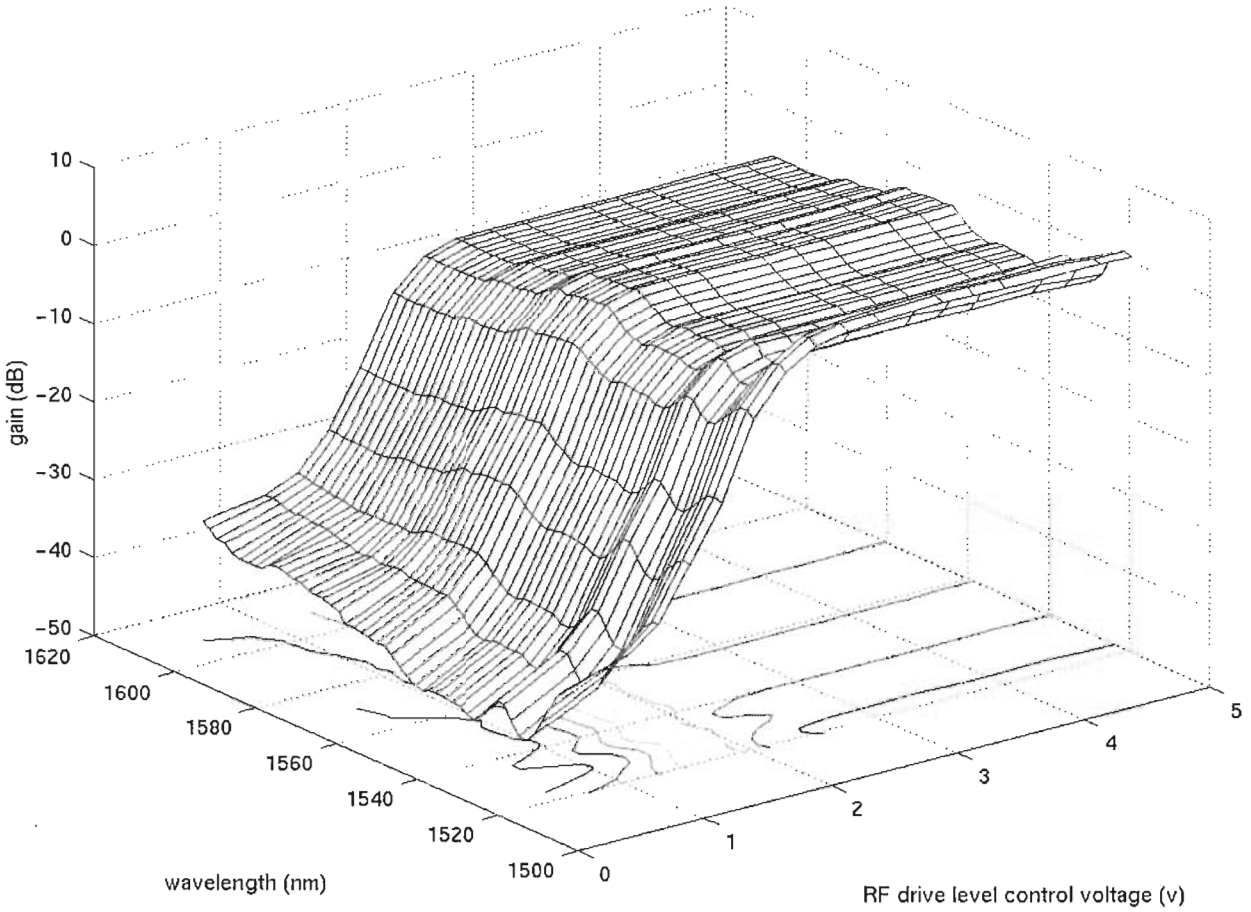

Fig. 25 Output spectrum of Super regenerative source

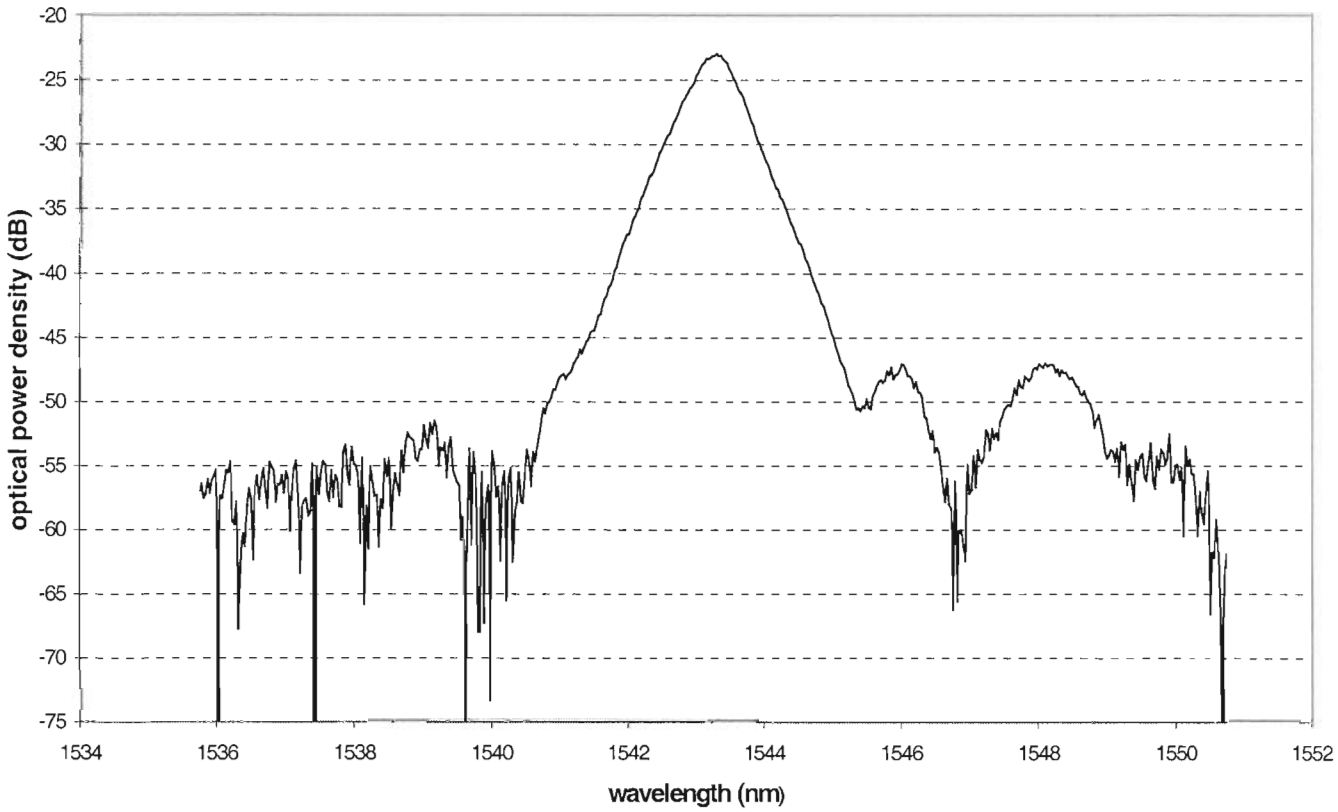

Figure 26. Super-luminescent source with single pass AOTF filtering.

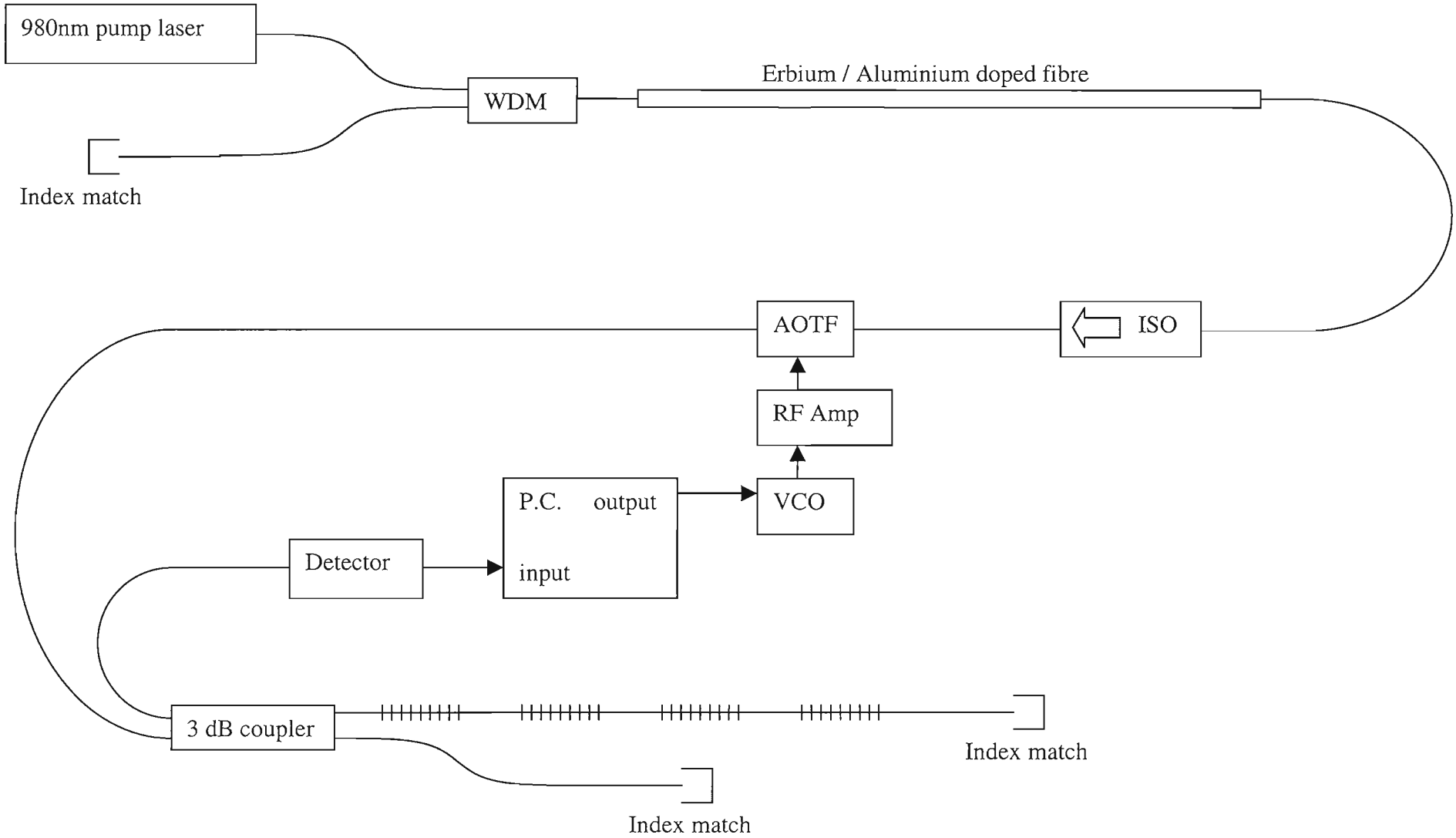

Figure 27. Super-luminescent source with double pass AOTF filtering.

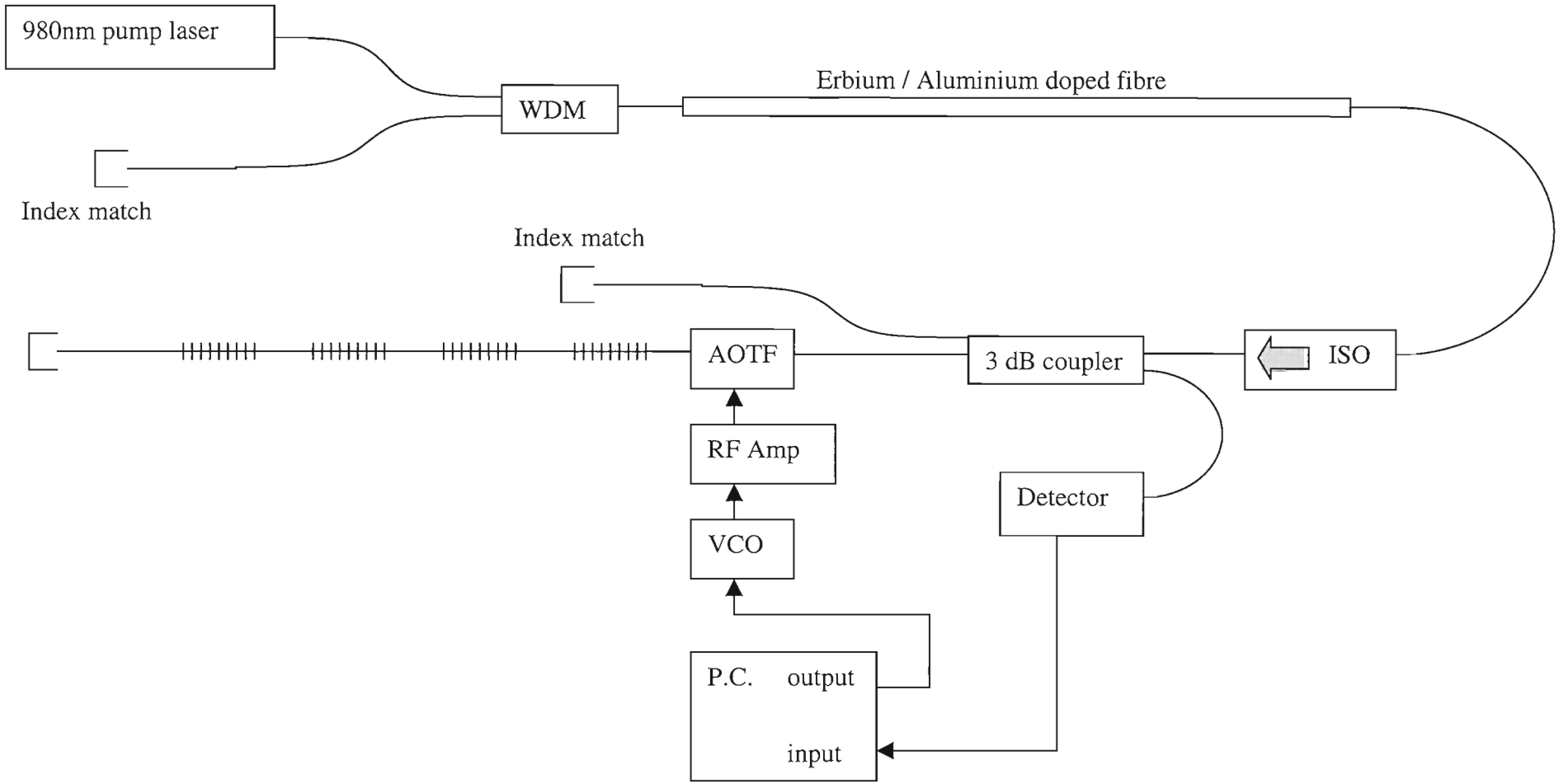

Figure 28. Configuration including a super regenerative source

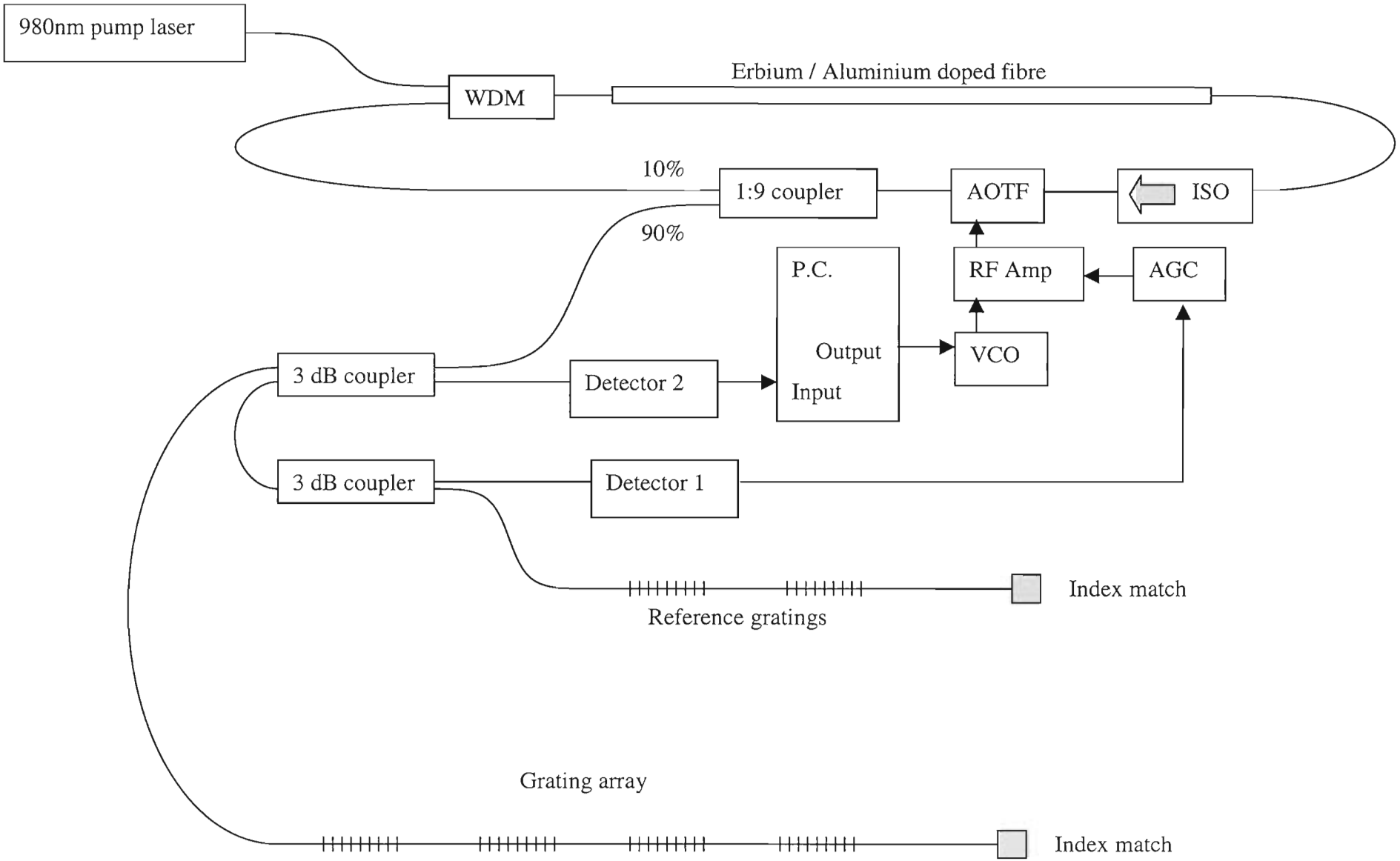

Figure 29. Double pass tuneable source.

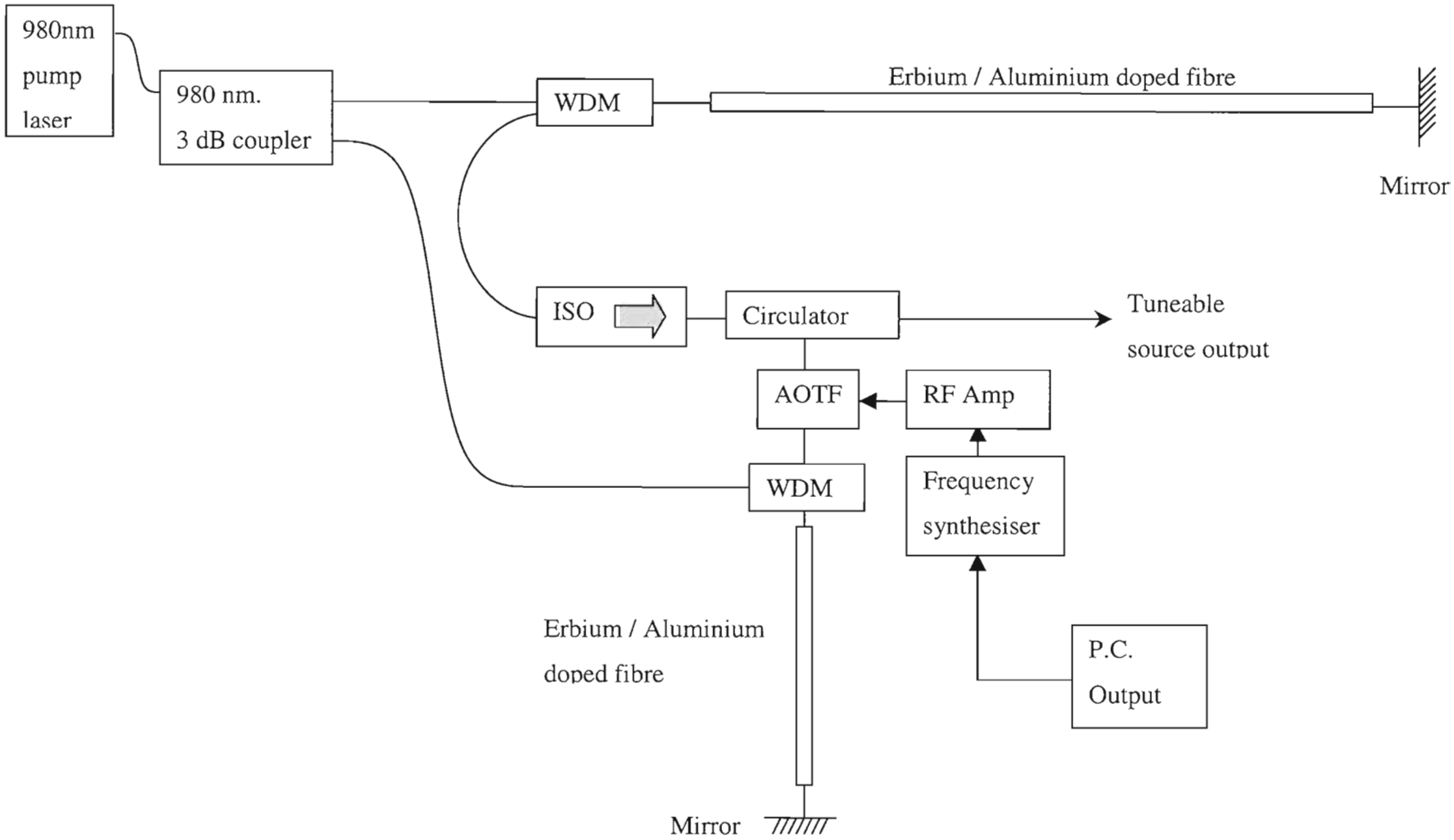

Figure 30. Active Gain Control Unit.

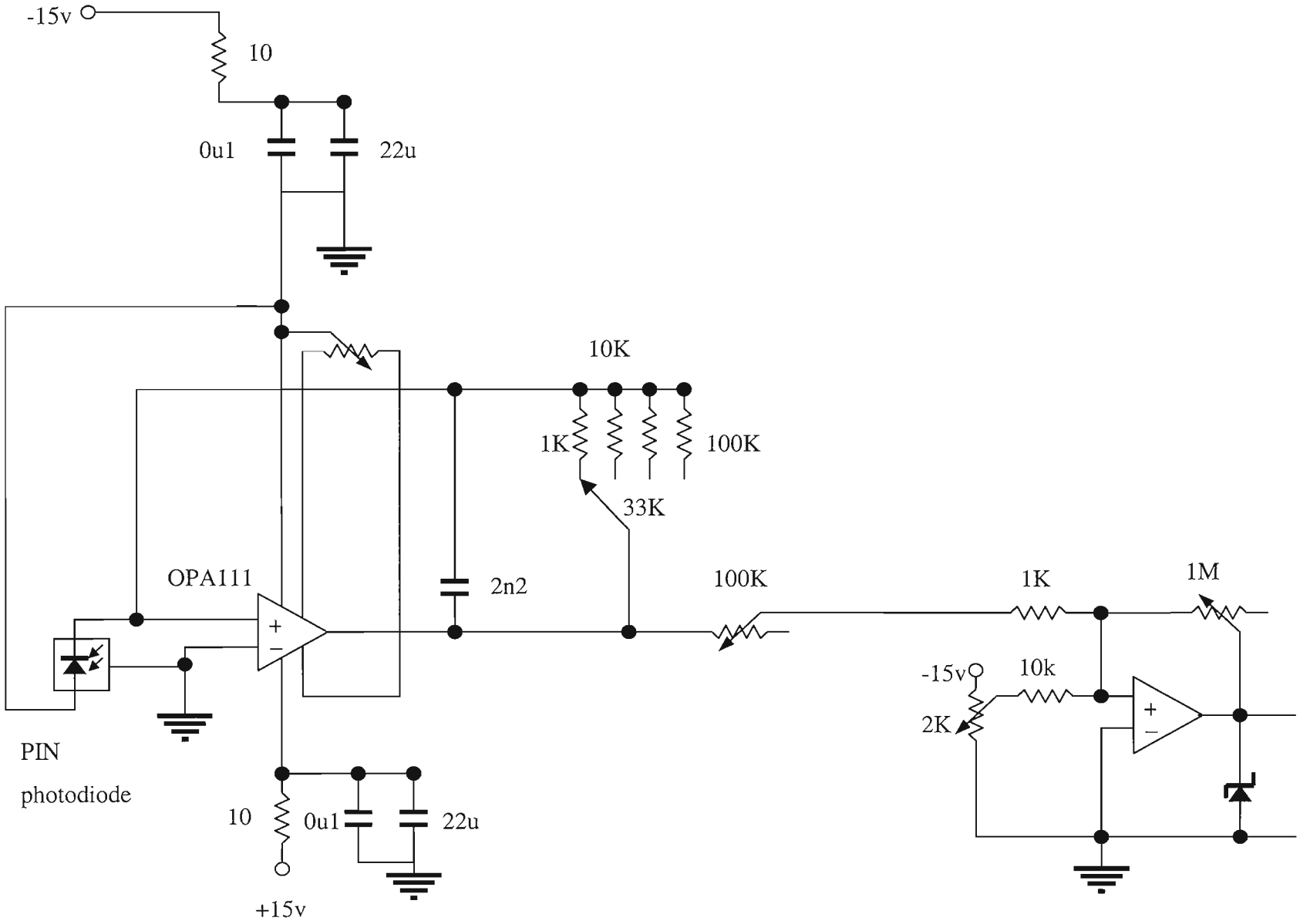

Figure 31. VCO circuit.

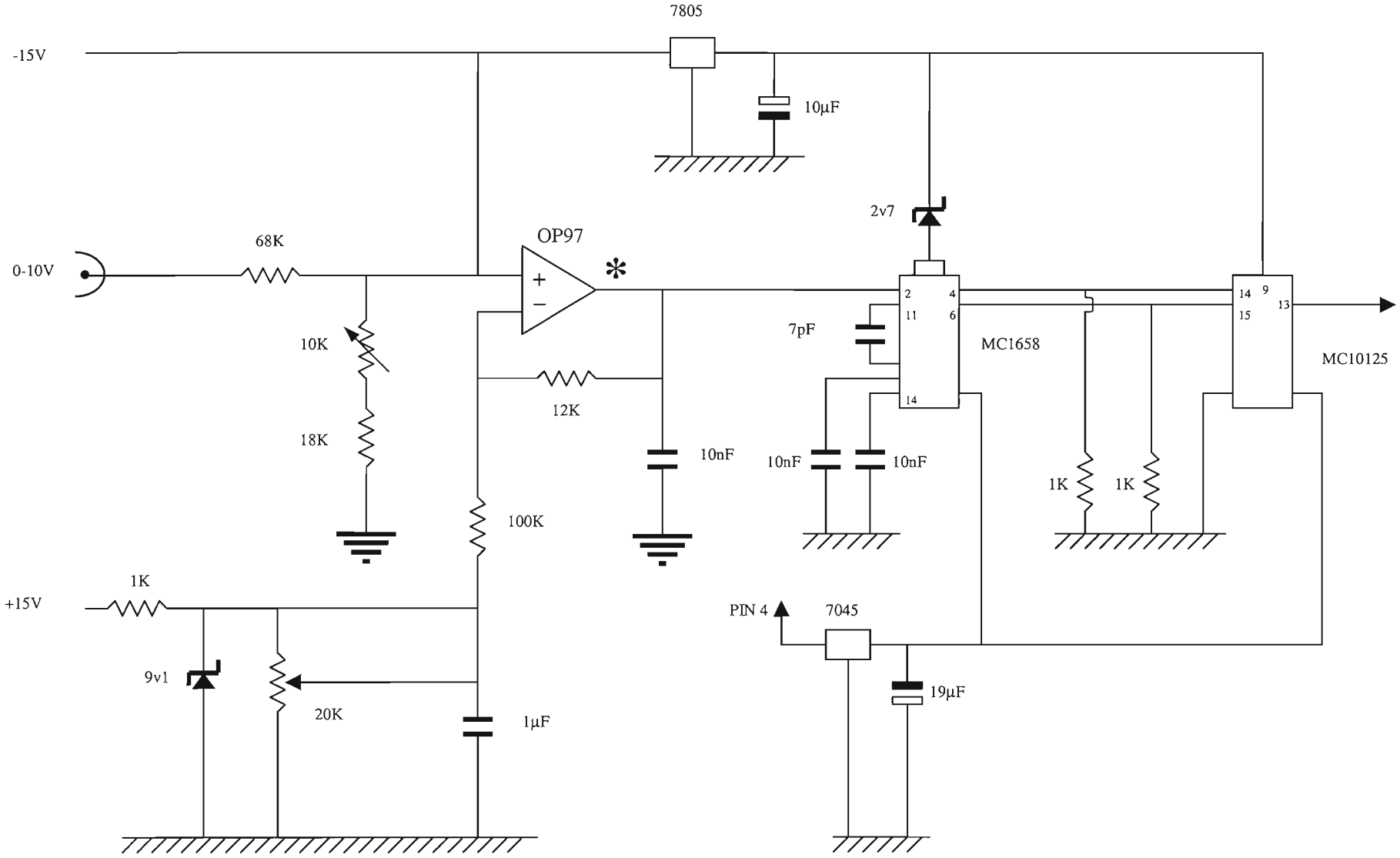

Fig 32. VCO calibration curves

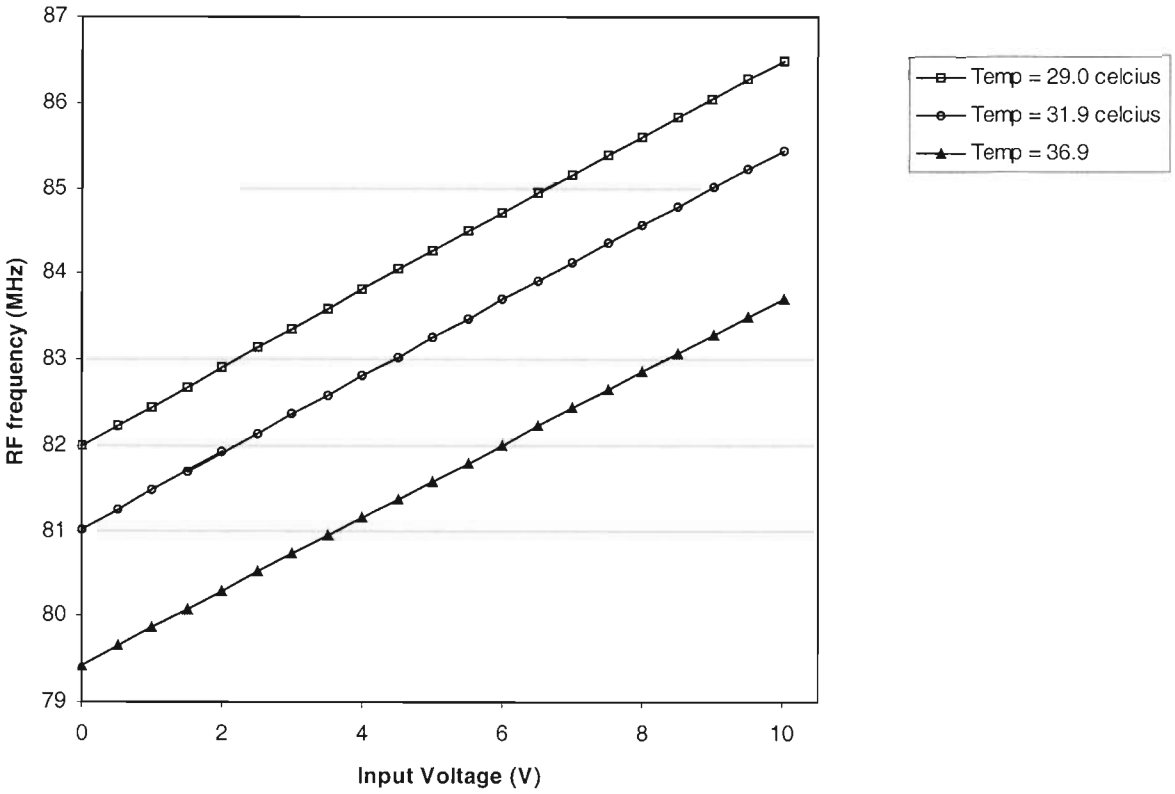

Figure 33. Spectral Sample points

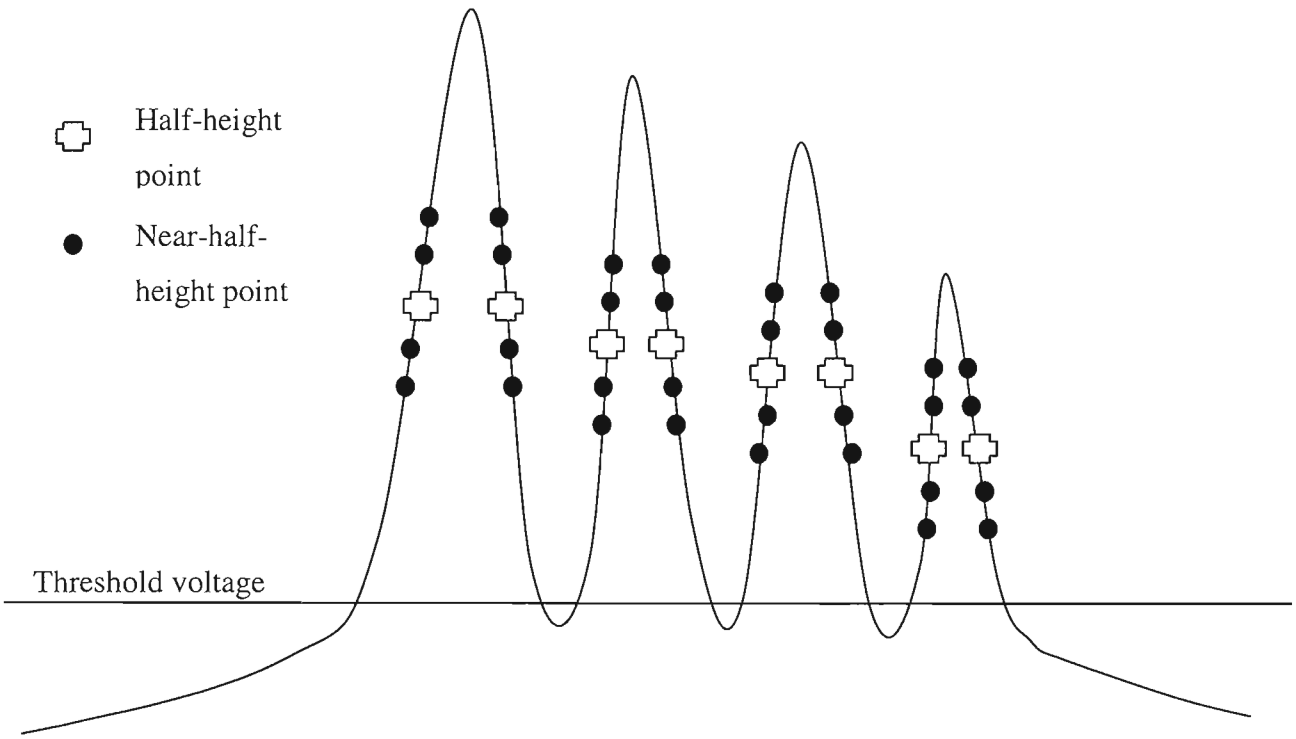

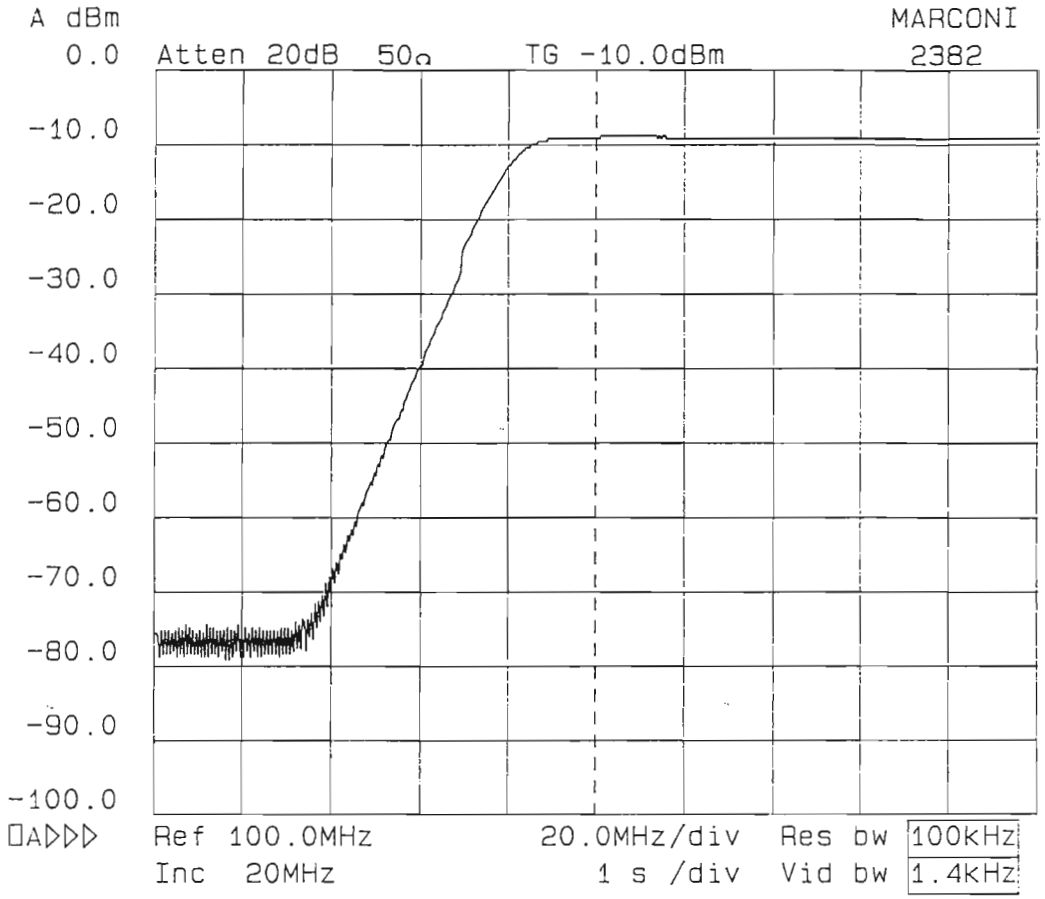

Fig. 34 Frequency response of 100MHz high pass filter

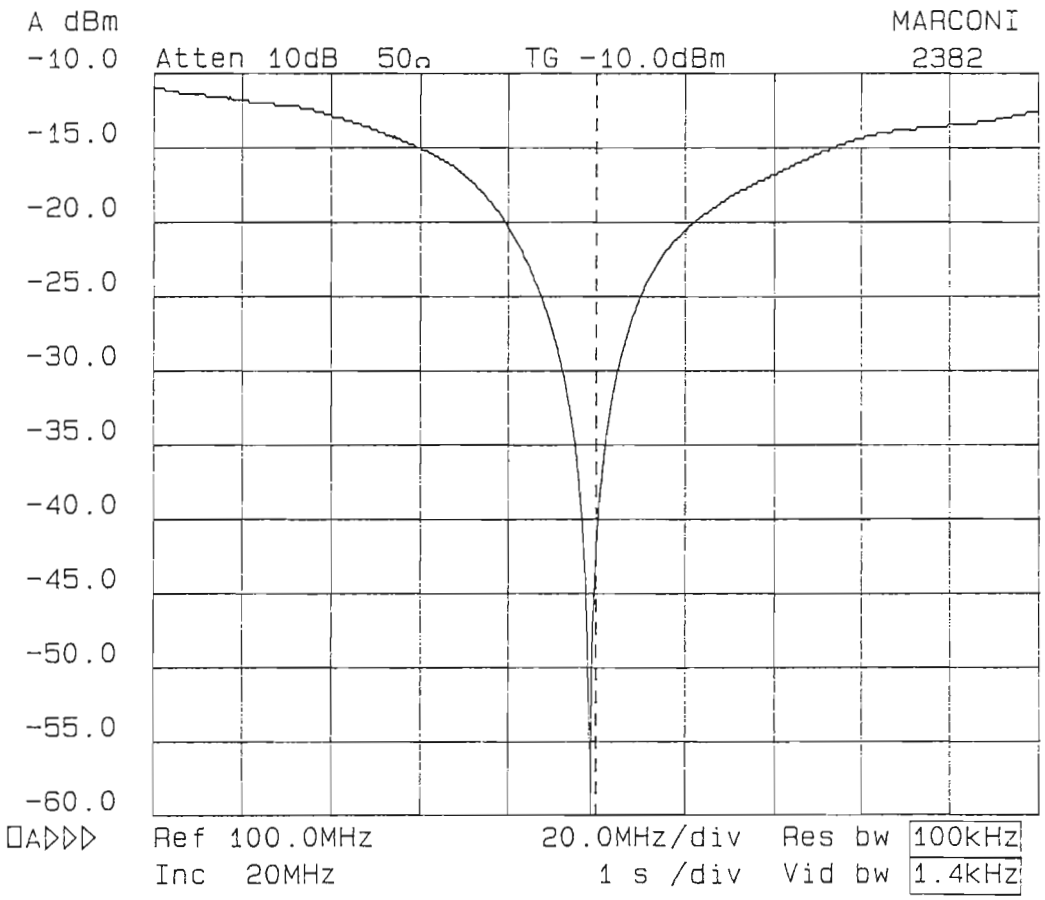

Fig 35 Frequency response of 100MHz notch filter

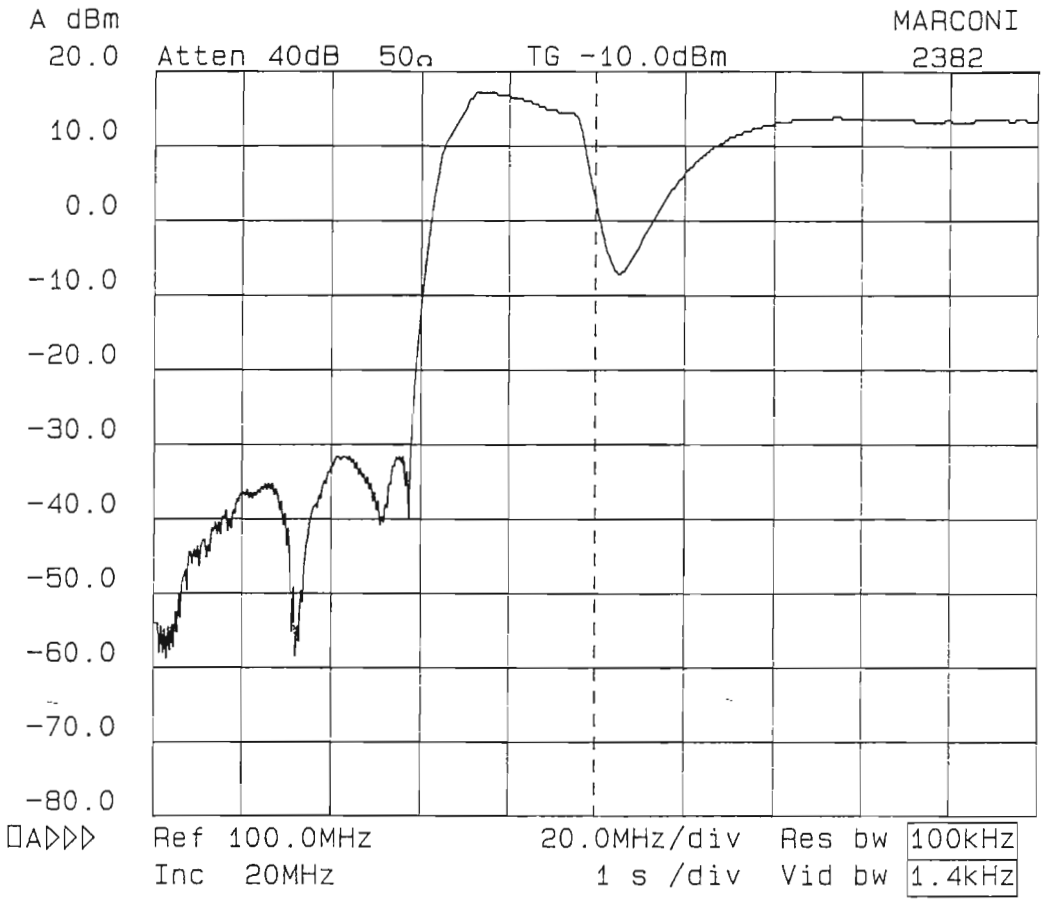

Fig 36 Frequency response of band pass filtration and amplification stage

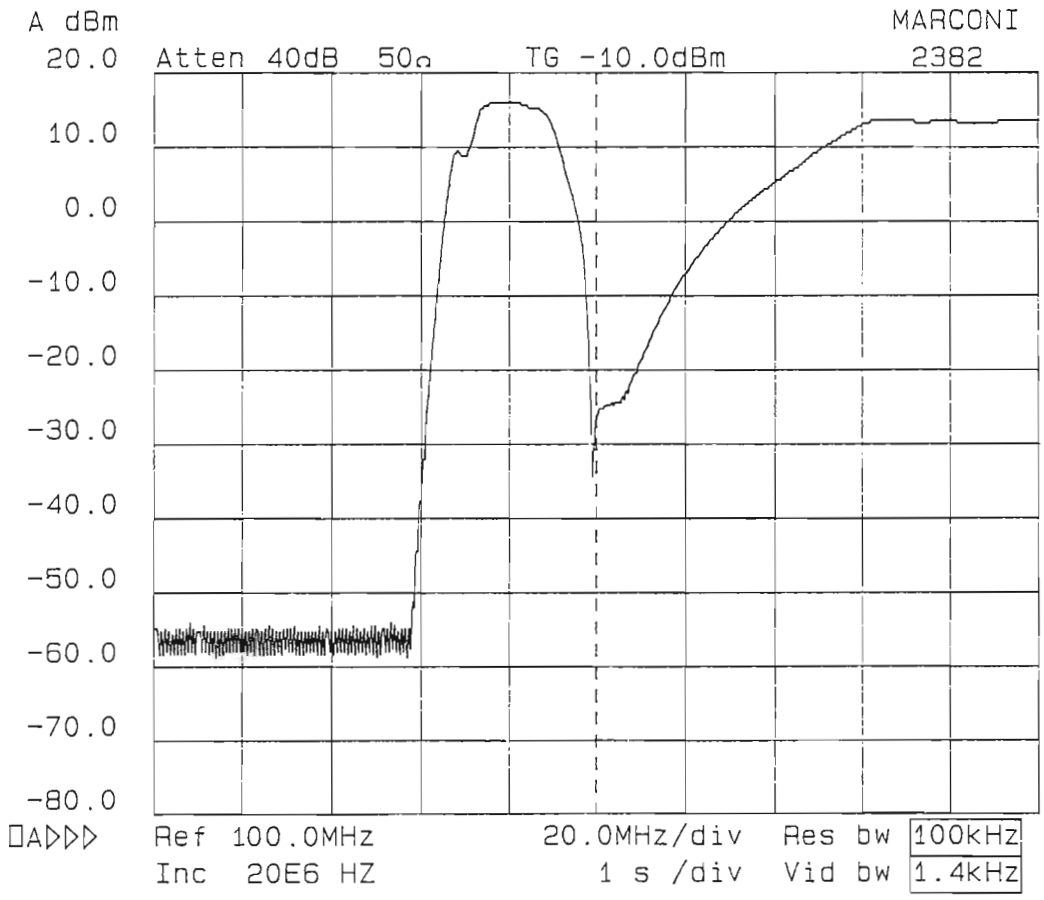

Fig 37 Frequency response of entire RF conditioning circuit

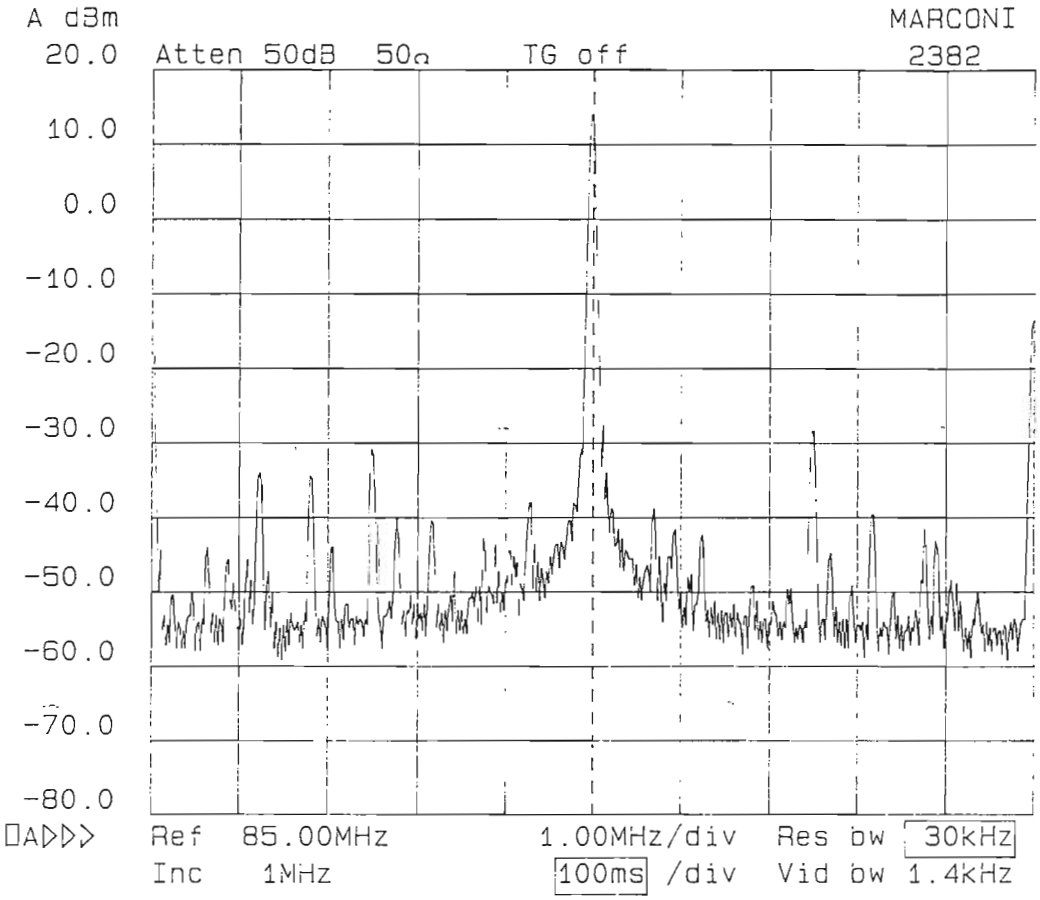

Fig 39 In-band output of RF circuit

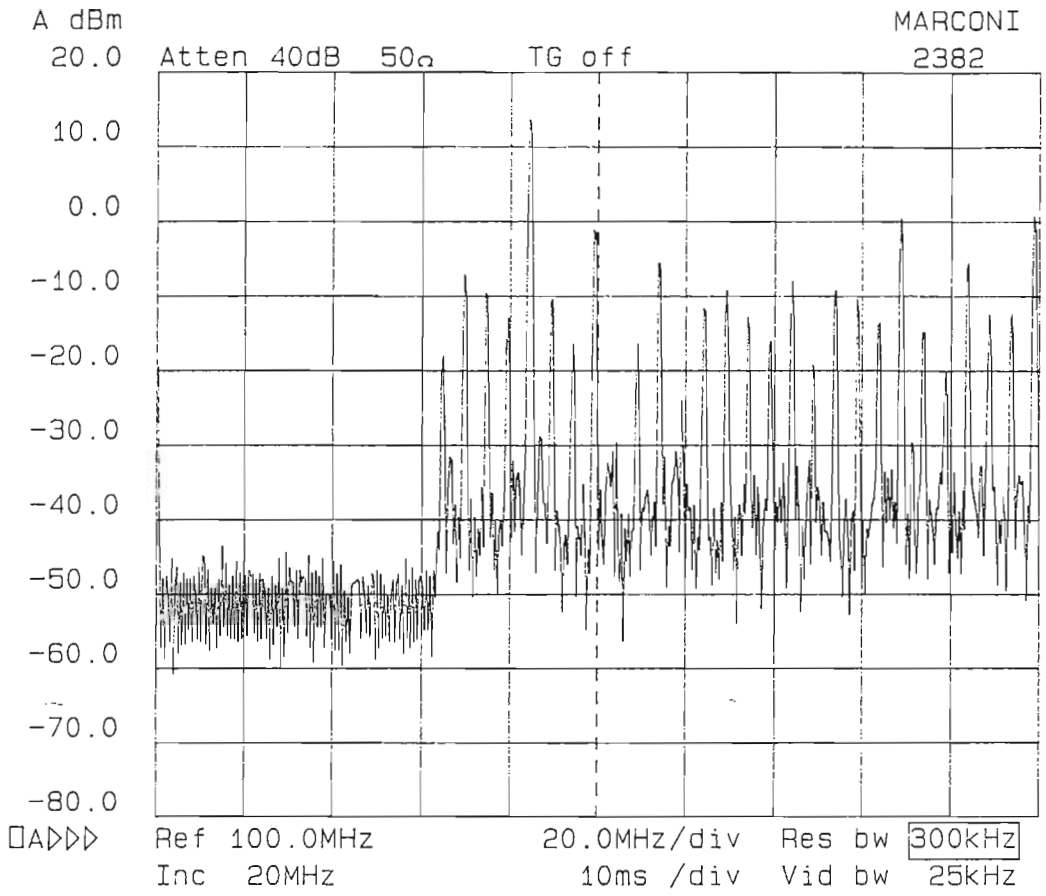

Fig 40 Output of RF circuit (wide scale)

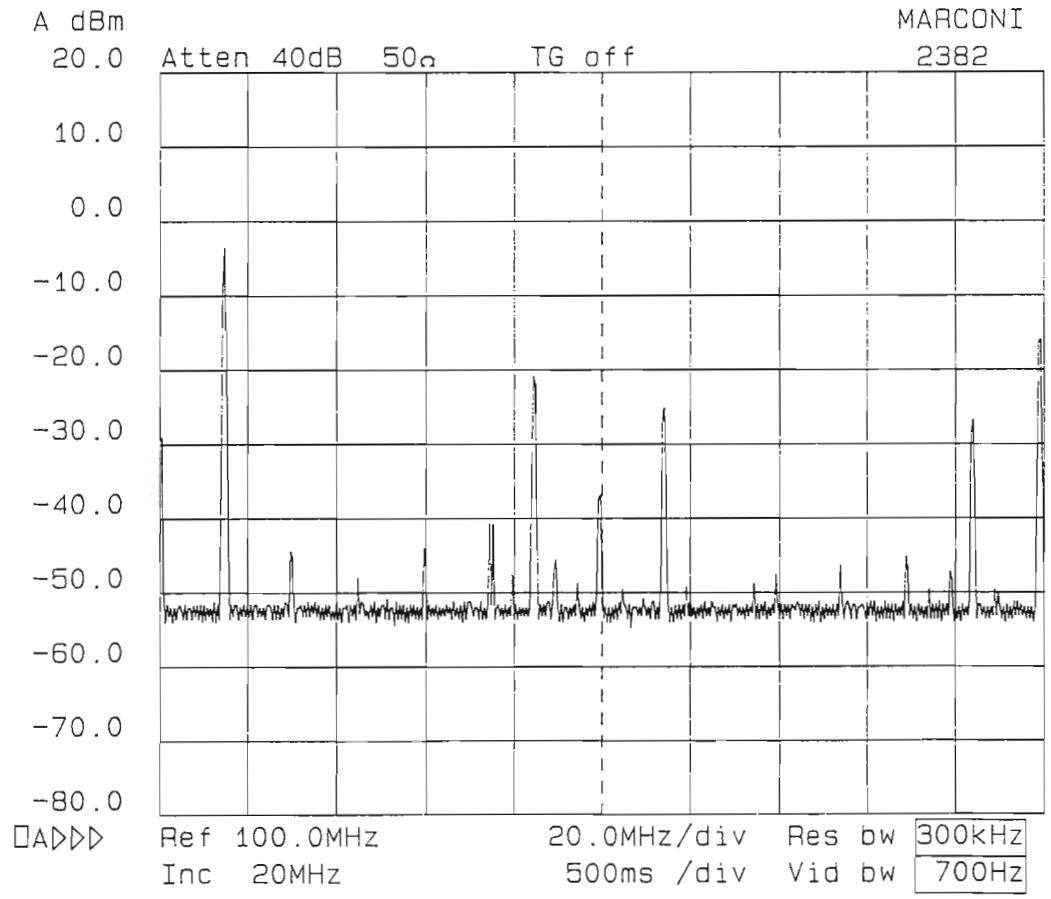

Fig 41 Output of frequency synthesiser

Fig. 42 Reference grating temperature controller